

Adjusting Posteriors from Composite and Misspecified Likelihoods with Application to Spatial Extremes in R-INLA

Silius M. Vandeskog

Department of Mathematics, The Norwegian University of Science and Technology (NTNU)

and

Sara Martino

Department of Mathematics, The Norwegian University of Science and Technology (NTNU)

and

Raphaël Huser

Statistics program, CEMSE Division, King Abdullah University of Science and Technology (KAUST)

October 4, 2022

Abstract

Methods such as low-rank approximations, covariance tapering and composite likelihoods are useful for speeding up inference in settings where the true likelihood is unknown or intractable to compute. However, such methods can lead to considerable model misspecification, which is particularly challenging to deal with and can provide misleading results when performing Bayesian inference. Adjustment methods for improving properties of posteriors based on composite and/or misspecified likelihoods have been developed, but these cannot be used in conjunction with certain computationally efficient inference software, such as the R-INLA package. We develop a novel adjustment method aimed at postprocessing posterior distributions to improve the properties of their credible intervals. The adjustment method can be used in conjunction with any software for Bayesian inference that allows for sampling from the posterior. Several simulation studies demonstrate that the adjustment method performs well in a variety of different settings. The method is also applied for performing improved modelling of extreme hourly precipitation from high-resolution radar data in Norway, using the spatial conditional extremes model and R-INLA. The results show a clear improvement in performance for all model fits after applying the posterior adjustment method.

Keywords: Model misspecification, Composite likelihoods, Bayesian inference, Spatial conditional extremes

1 Introduction

Bayesian modelling of high-dimensional spatial and/or temporal data has attracted much attention in recent decades, see, e.g., Diggle et al. (1998), Banerjee et al. (2014) and Gelfand et al. (2010) for a non-extensive list of methods and applications. Likelihood-based inference for such high-dimensional models is challenging and often computationally intractable. When inference is intractable the modeller has two choices: Either switch to a more efficient inference method or adjust the model into one with similar properties but lower computational cost. The first choice is often preferred, as typically the model was chosen for a good reason. Methods that help speed up Bayesian inference include approximate Bayesian computation (ABC) methods (Marin et al., 2012; Sisson et al., 2018), Max-and-Smooth methods (Hrafnkelsson et al., 2021; Jóhannesson et al., 2022), improved Markov chain Monte Carlo (MCMC) methods such as Hamiltonian Monte Carlo, with efficient implementations in the `Stan` software (Carpenter et al., 2017), and the integrated nested Laplace approximation (INLA; Rue et al., 2009) with efficient implementations in the `R-INLA` package for the `R` programming language (Rue et al., 2017). INLA has become very popular thanks to its combination of computational efficiency and high accuracy. Based on deterministic numerical approximations of the posterior distribution, the method can be applied for inference on latent Gaussian models, which are popular and commonly used in a large variety of applications, including high-dimensional spatial and/or temporal modelling (Lombardo et al., 2020; Opitz et al., 2022; E. S. Simpson et al., 2020).

When inference is intractable even with improved inference methods like the aforementioned, it is necessary to change the model itself. As an example, high-dimensional spatial and/or temporal phenomena are often modelled using (possibly transformed) Gaussian processes, not necessarily because they are believed to be exactly Gaussian, but because Gaussian processes are a rather flexible class of models that are computationally efficient with appealing theoretical properties (e.g., Banerjee et al., 2014). Gaussian processes are even applied in settings where they are known in advance to provide a misspecified representation of the true data generating process, because alternative models may be too complex or computationally intensive to fit (Davison et al., 2012; Vandeskog et al., 2022). However, inference for Gaussian processes typically requires computing the inverse of the covariance matrix, whose cost scales cubically with the model dimension. Thus, in truly high-dimensional problems, even inference based on Gaussian processes becomes intractable.

A common approach for further speeding up inference is to enforce (realistic or artificial) assumptions of conditional or unconditional independence that lead to simplified likelihood expressions. Covariance tapering, low-rank estimation and composite likelihoods are all based on this approach. Covariance tapering (Kaufman et al., 2008) relies on the working assumption that random variables become independent beyond a specified distance. This leads to sparse covariance matrices that are easier to invert. Low-rank estimation is based on approximating random processes with linear combinations of lower-dimensional processes, leading to low-rank covariance matrices that are easier to deal with computationally. The list

of low-rank approximation methods includes predictive process models (Banerjee et al., 2008), fixed-rank Kriging (Cressie & Johannesson, 2008) and models based on stochastic partial differential equations (SPDE; Lindgren et al., 2011). Composite likelihoods are functions composed of many lower-dimensional likelihoods (Lindsay, 1988), which may completely remove the need to invert any high-dimensional covariance matrices. The class of composite likelihoods includes the independence likelihood (Chandler & Bate, 2007), the pairwise likelihood (Cox & Reid, 2004), the block likelihood (Eidsvik et al., 2014) and the Vecchia approximation (Vecchia, 1988), among others. A composite likelihood must be treated carefully as, in general, it does not correspond to the likelihood of a proper statistical model. However, the theory on composite likelihoods is well developed, and corresponding maximum composite likelihood estimators have been shown to perform well both in theory and in practice (Varin et al., 2011).

A common challenge with all methods above is that they often introduce large amounts of model misspecification through unrealistic distributional assumptions. While composite likelihoods are not valid likelihood functions, they have a lot in common with misspecified likelihoods, as shown in Section 2, and in this paper we consider composite likelihoods as a type of misspecified likelihoods. Misspecified likelihoods complicate Bayesian inference and can result in posterior distributions with poor frequency properties, meaning that, as the sample size increases and the prior loses all influence, $(1 - \alpha)$ -credible intervals do not, in general, coincide with $(1 - \alpha)$ -confidence intervals (Kleijn & van der Vaart, 2012; Ribatet et al., 2012). Adjustments for improving the properties of posterior credible intervals have been proposed by, e.g., Chandler and Bate (2007), Pauli et al. (2011), Ribatet et al. (2012), and Syring and Martin (2018). Unfortunately, all such adjustments require specific modifications of the likelihood function. Therefore, they usually cannot be used in conjunction with optimised software for Bayesian inference, such as R-INLA, where the user must choose from a predefined list of likelihood functions that cannot be modified. In this paper, we develop a novel method for improving the frequency properties of a posterior distribution, based on postprocessing posterior samples. This method can be applied to a broad class of computational software, including R-INLA.

We apply our method to the spatial conditional extremes model (Wadsworth & Tawn, 2022), and use it to study spatial extreme precipitation from a high-resolution dataset. Inference for this model traditionally relies on composite likelihoods, not for computational efficiency, but for using more data for estimation. In recent years, this modelling framework has gained much traction in the field of extreme value theory, as it allows for a more flexible description of extremal dependence than classical extreme value models (Huser & Wadsworth, 2022). The model consists in choosing one spatial location and modelling surrounding data conditional on extreme behaviour at that site. As extreme behaviour is, by definition, rare, inference commonly relies on a composite likelihood that combines separate models from multiple conditioning sites in order to provide one global model fit that, on average, represents the data well for any given conditioning site (Heffernan & Tawn, 2004; Richards et al., 2022; E. S. Simpson & Wadsworth, 2021; Wadsworth & Tawn, 2022). A modification of the spatial

conditional extremes model implemented in R-INLA is proposed by E. S. Simpson et al. (2020) in order to perform truly high-dimensional Bayesian inference using INLA and the SPDE approach. The authors only employ single site conditioning, stating that their reason for not providing a global model fit comes from the problems that occur when performing Bayesian inference with a composite likelihood using R-INLA. We demonstrate that our adjustment method solves these problems and allows for a global Bayesian model fit with improved frequency properties. We also improve upon parts of the model construction proposed by Wadsworth and Tawn (2022) and E. S. Simpson et al. (2020), and we demonstrate a general methodology for implementing different variants of the conditional extremes model in R-INLA using the recent `cgeneric` framework.

The remainder of the paper is organised as follows: In Section 2, we examine problems that can occur when performing Bayesian inference based on composite and/or misspecified likelihoods. Previous adjustment methods are presented, and our novel method for post-processing posteriors is developed. The spatial conditional extremes model and inferential methods based on composite likelihoods are reviewed in Section 3. There, we also build upon E. S. Simpson et al. (2020) for improving how such models can be implemented in R-INLA. Section 4 contains several simulation studies for evaluating both the adjustment method and our conditional extremes model implementation in R-INLA. Section 5 contains a case study where the spatial conditional extremes model and the posterior adjustment method are used for modelling extreme precipitation from high-resolution radar data in Norway. Finally, we conclude in Section 6 with some discussion and perspectives on future research.

2 Methodology

2.1 Inference with composite and/or misspecified likelihoods

Let $\mathbf{y} \in \mathbb{R}^d$ be a realisation of a random vector \mathbf{Y} with distribution function G , and assume that one models the data \mathbf{y} using the parametric family $\mathcal{F} = \{F(\cdot; \boldsymbol{\theta}) : \boldsymbol{\theta} \in \Theta\}$. If G is not contained in \mathcal{F} , we say that \mathcal{F} is misspecified. Denote the likelihood function corresponding to $F(\cdot; \boldsymbol{\theta})$ as $L(\boldsymbol{\theta}; \cdot)$. Lindsay (1988) defines composite likelihoods as functions composed of likelihood functions of conditional or marginal events for \mathbf{y} . Thus, given a set of events $A_1, A_2, \dots, A_m, B_1, B_2, \dots, B_m \subseteq \mathbb{R}^d$ and nonnegative weights $\omega_1, \omega_2, \dots, \omega_m \geq 0$, a composite likelihood is defined as the weighted product

$$L_c(\boldsymbol{\theta}; \mathbf{y}) = \prod_{i=1}^m L^{(i)}(\boldsymbol{\theta}; \mathbf{y})^{\omega_i}, \text{ where } L^{(i)}(\boldsymbol{\theta}; \mathbf{y}) = L(\boldsymbol{\theta}; [\mathbf{y} \in A_i \mid \mathbf{y} \in B_i]),$$

Given n independent realisations $\mathcal{Y} = \{\mathbf{y}_1, \dots, \mathbf{y}_n\}$ of \mathbf{Y} , the composite log-likelihood equals

$$\ell_c(\boldsymbol{\theta}; \mathcal{Y}) = \sum_{j=1}^n \ell_c(\boldsymbol{\theta}; \mathbf{y}_j) = \sum_{j=1}^n \sum_{i=1}^m \omega_{ij} \log L^{(i)}(\boldsymbol{\theta}; \mathbf{y}_j) = \sum_{j=1}^n \sum_{i=1}^m \omega_{ij} \ell^{(i)}(\boldsymbol{\theta}; \mathbf{y}_j), \quad (1)$$

where we allow for different weights for different realisations of \mathbf{Y} . Incorrectly interpreting the composite likelihood as a true likelihood is tantamount to specifying a model for \mathcal{Y} using a family of distributions in which $[\mathbf{y}_i \in A_j \mid \mathbf{y}_i \in B_j]$ is (wrongly) assumed to be independent of $[\mathbf{y}_i \in A_k \mid \mathbf{y}_i \in B_k]$ for all i and $j \neq k$. One can therefore consider a composite likelihood as a type of misspecified model with unrealistic independence assumptions. From (1) it is clear that any proper likelihood is a composite likelihood with $m = 1$ and $\omega_1 = 1$. Consequently, all the theory of composite likelihoods trivially holds for valid likelihoods.

Using the theory of unbiased estimating equations one can show that the maximum composite likelihood estimator, $\hat{\boldsymbol{\theta}}_c = \arg \max_{\boldsymbol{\theta}} \ell_c(\boldsymbol{\theta}; \mathcal{Y})$, is asymptotically Gaussian distributed,

$$\mathcal{I}(\boldsymbol{\theta}^*)^{1/2} \left(\hat{\boldsymbol{\theta}}_c - \boldsymbol{\theta}^* \right) \rightsquigarrow \mathcal{N}(\mathbf{0}, \mathbf{I}), \text{ as } n \rightarrow \infty,$$

under some weak regularity conditions (White, 1982), where \mathbf{I} is the identity matrix and $\boldsymbol{\theta}^*$ is the minimiser of the Kullback-Leibler distance (KLD; Kullback & Leibler, 1951) between the likelihood of the true distribution G and the composite likelihood L_c . Furthermore, $\mathcal{I}(\boldsymbol{\theta})$ is the so-called Godambe sandwich information matrix (Godambe, 1960):

$$\begin{aligned} \mathcal{I}(\boldsymbol{\theta}) &= \mathbf{H}(\boldsymbol{\theta}) \mathbf{J}(\boldsymbol{\theta})^{-1} \mathbf{H}(\boldsymbol{\theta}), \\ \mathbf{H}(\boldsymbol{\theta}) &= -\mathbb{E} [\nabla_{\boldsymbol{\theta}}^2 \ell_c(\boldsymbol{\theta}; \mathcal{Y})], \quad \mathbf{J}(\boldsymbol{\theta}) = \text{Cov} (\nabla_{\boldsymbol{\theta}} \ell_c(\boldsymbol{\theta}; \mathcal{Y})), \end{aligned} \tag{2}$$

where expectations are taken with respect to G . If the composite likelihood is a valid and correctly specified likelihood then $\mathbf{H}(\boldsymbol{\theta}^*) = \mathbf{J}(\boldsymbol{\theta}^*)$ and the Godambe sandwich information is reduced to the Fisher information $\mathcal{I}(\boldsymbol{\theta}^*) = \mathbf{H}(\boldsymbol{\theta}^*) = \mathbf{J}(\boldsymbol{\theta}^*)$.

Given a prior distribution $\pi(\boldsymbol{\theta})$ for $\boldsymbol{\theta}$, and a composite likelihood $L_c(\boldsymbol{\theta}; \cdot)$ such that $\int_{\Theta} L_c(\boldsymbol{\theta}; \mathcal{Y}) \pi(\boldsymbol{\theta}) d\boldsymbol{\theta}$ is finite, the posterior distribution of $[\boldsymbol{\theta} \mid \mathcal{Y}]$ is defined as

$$\pi_c(\boldsymbol{\theta} \mid \mathcal{Y}) = \frac{L_c(\boldsymbol{\theta}; \mathcal{Y}) \pi(\boldsymbol{\theta})}{\int_{\Theta} L_c(\boldsymbol{\theta}; \mathcal{Y}) \pi(\boldsymbol{\theta}) d\boldsymbol{\theta}}.$$

Under appropriate regularity conditions, this distribution converges asymptotically to a Gaussian distribution with mean $\boldsymbol{\theta}^*$ and covariance matrix $\mathbf{H}(\boldsymbol{\theta}^*)^{-1}$ (Berk, 1966; Kleijn & van der Vaart, 2012; Ribatet et al., 2012). Notice that the asymptotic covariance of the posterior is different from the asymptotic covariance of the maximum likelihood estimator, with equality only when the composite likelihood is a valid and correctly specified likelihood. This causes the posterior to lose its frequency properties when $L_c(\boldsymbol{\theta}; \cdot)$ is misspecified. Consequently, care must always be taken when interpreting credible intervals that are based on composite likelihoods or other types of clearly misspecified models.

Adjustments to the composite likelihood have been proposed for improving its frequency properties. Pauli et al. (2011) and Ribatet et al. (2012) propose to rescale the weights ω_{ij} in (1) so that the composite and the true likelihood ratio statistics achieve the same distribution asymptotically. Syring and Martin (2018) also rescale ω_{ij} , using bootstrap techniques to estimate the best rescaling value. Chandler and Bate (2007) and Ribatet et al. (2012) propose an affine transformation to the argument of the composite likelihood,

$$L_{\text{adj}}(\boldsymbol{\theta}; \mathcal{Y}) = L_c(\boldsymbol{\theta}^* + \mathbf{C}(\boldsymbol{\theta} - \boldsymbol{\theta}^*); \mathcal{Y}), \tag{3}$$

where the matrix \mathbf{C} is a solution of the equation $\mathbf{C}^T \mathbf{H}(\boldsymbol{\theta}^*) \mathbf{C} = \mathbf{I}(\boldsymbol{\theta}^*)$, with $\mathbf{I}(\boldsymbol{\theta})$ and $\mathbf{H}(\boldsymbol{\theta})$ as defined in (2). All of the aforementioned methods are based on modifying the likelihood function before performing inference. However, this option is not available for users of inference software like R-INLA, where one must choose between a preselected set of likelihood functions. Therefore, in Section 2.2, we develop a novel adjustment method for posterior distributions based on composite and/or misspecified likelihoods that can be used in conjunction with any Bayesian inference program, including R-INLA.

2.2 Postprocessing posterior samples

Inspired by Chandler and Bate (2007) and Ribatet et al. (2012), we propose an affine transformation for samples from the posterior distribution, aimed at improving the frequency properties of credible intervals. Assume that the parameter $\boldsymbol{\theta}$ is sampled from a posterior distribution based on a composite and/or misspecified likelihood. We then define the adjusted version of $\boldsymbol{\theta}$ as

$$\boldsymbol{\theta}_{\text{adj}} = \boldsymbol{\theta}^* + \mathbf{C}(\boldsymbol{\theta} - \boldsymbol{\theta}^*), \quad (4)$$

where the matrix \mathbf{C} is chosen such that the asymptotic distribution of $\boldsymbol{\theta}_{\text{adj}}$ as $n \rightarrow \infty$ is Gaussian with mean $\boldsymbol{\theta}^*$ and covariance matrix $\mathbf{I}(\boldsymbol{\theta}^*)^{-1}$. To achieve this, \mathbf{C} must solve the equation $\mathbf{C} \mathbf{H}(\boldsymbol{\theta}^*)^{-1} \mathbf{C}^T = \mathbf{I}(\boldsymbol{\theta}^*)^{-1}$. A solution of this equation is

$$\mathbf{C} = (\mathbf{M}_1^{-1} \mathbf{M}_2)^T, \text{ with } \mathbf{M}_1^T \mathbf{M}_1 = \mathbf{H}(\boldsymbol{\theta}^*)^{-1} \text{ and } \mathbf{M}_2^T \mathbf{M}_2 = \mathbf{I}(\boldsymbol{\theta}^*)^{-1},$$

where the matrix square roots \mathbf{M}_1 and \mathbf{M}_2 are computed using, e.g., singular value decomposition. Notice that our \mathbf{C} matrix is different from the \mathbf{C} matrix of Chandler and Bate (2007) and Ribatet et al. (2012) in (3), since we solve a slightly different equation.

In order to estimate \mathbf{C} one must first estimate the values of $\boldsymbol{\theta}^*$, $\mathbf{H}(\boldsymbol{\theta}^*)$ and $\mathbf{J}(\boldsymbol{\theta}^*)$. The mode of the likelihood, $\boldsymbol{\theta}^*$, can be estimated by the mode of the posterior $\pi_c(\boldsymbol{\theta} \mid \mathcal{Y})$, denoted $\hat{\boldsymbol{\theta}}^*$. The estimator $\hat{\boldsymbol{\theta}}^*$ provides a good approximation to $\boldsymbol{\theta}^*$ if the prior is not overly informative and the sample size is large enough, but other estimators may be more suitable if this does not hold. The first step towards estimating $\mathbf{J}(\boldsymbol{\theta}^*)$ is to compute the gradients $\nabla_{\boldsymbol{\theta}} \ell^{(i)}(\hat{\boldsymbol{\theta}}^*; \mathbf{y}_j)$ for $i = 1, 2, \dots, m$ and $j = 1, 2, \dots, n$. These can be computed analytically or estimated using numerical derivation methods. Having computed all the gradients, we estimate $\mathbf{J}(\boldsymbol{\theta}^*)$ with

$$\hat{\mathbf{J}}(\hat{\boldsymbol{\theta}}^*) = \sum_{i,j} \omega_{ij} \nabla_{\boldsymbol{\theta}} \ell^{(i)}(\hat{\boldsymbol{\theta}}^*; \mathbf{y}_j) \sum_{(i',j') \in \Delta(i,j)} \omega_{i'j'} \left(\nabla_{\boldsymbol{\theta}} \ell^{(i')}(\hat{\boldsymbol{\theta}}^*; \mathbf{y}_{j'}) \right)^T, \quad (5)$$

where $\Delta(i, j)$ is the set of neighbours to (i, j) in the sense that $(i', j') \in \Delta(i, j)$ if and only if $\nabla_{\boldsymbol{\theta}} \ell^{(i')}(\cdot; \mathbf{y}_{j'})$ is correlated with $\nabla_{\boldsymbol{\theta}} \ell^{(i)}(\cdot; \mathbf{y}_j)$. Summing over all the non-correlated pairs of tuples would introduce unnecessary noise that could cause the estimator to approximately equal zero (Lumley & Heagerty, 1999). In practice one can therefore often compute $\hat{\mathbf{J}}(\hat{\boldsymbol{\theta}}^*)$ using a sliding window approach.

Estimation of $\mathbf{H}(\boldsymbol{\theta}^*)$ is often easier than that of $\mathbf{J}(\boldsymbol{\theta}^*)$, since the former is a matrix of expected values, whereas the latter is a covariance matrix. The law of large number implies that, for n and m large enough, a good estimator for $\mathbf{H}(\boldsymbol{\theta}^*)$ is

$$\hat{\mathbf{H}}(\hat{\boldsymbol{\theta}}^*) = - \sum_{j=1}^n \sum_{i=1}^m \omega_{ij} \nabla_{\boldsymbol{\theta}}^2 \ell^{(i)}(\hat{\boldsymbol{\theta}}^*; \mathbf{y}_j). \quad (6)$$

Thus, all we need for estimating $\mathbf{H}(\boldsymbol{\theta}^*)$ is to compute the Hessian of the composite log-likelihood terms at $\hat{\boldsymbol{\theta}}^*$. For users of R-INLA, this is especially simple, as an estimator of $\mathbf{H}(\hat{\boldsymbol{\theta}}^*)^{-1}$ is computed and returned by the program when fitting a model to data.

3 The spatial conditional extremes model

Having developed an adjustment method for posterior samples based on composite and/or misspecified likelihoods, we aim to perform Bayesian inference for the spatial conditional extremes model using a combination of R-INLA and a composite likelihood. The model is described in Section 3.1, while Section 3.2 details how to perform inference based on single site conditioning, and how to further improve it using a composite likelihood.

3.1 Model description

Statistical models for spatial extremes are crucial for properly assessing risks in a variety of applications, see Huser and Wadsworth (2022) for a non-extensive list of use-cases. An important component of spatial extreme value theory is the description and characterisation of a spatial process' extremal dependence properties. Two locations that have a positive limiting probability to experience extremes simultaneously are denoted extremally dependent. If this limiting probability is zero, the locations are denoted extremally independent. Clearly, simultaneous extreme precipitation over a large area has more dire consequences than extreme precipitation at one single point in space. Therefore, correct estimation of extremal dependence properties is of utmost importance when estimating environmental risks. Most of the classical models within spatial extreme value theory are either based on max-stable processes (e.g., Davison et al., 2019) or latent Gaussian models with conditional independence assumptions (e.g., Davison et al., 2012; Opitz et al., 2018). The latent Gaussian models often capture the marginal structure of spatial processes well, and are computationally efficient. However, due to common assumptions of conditional independence, they fail to properly describe extremal dependence properties. Max-stable processes are based on strong mathematical theory and allow for rich modelling of extremal dependence, but in practice they are often too computationally demanding and yield unsatisfactory models for extremal independence (Huser & Wadsworth, 2022). In recent years the conditional extremes model (Heffernan & Resnick, 2007; Heffernan & Tawn, 2004; Wadsworth & Tawn, 2022) has gained much traction, as it allows for a more flexible description of extremal dependence by modelling the behaviour of a random vector conditional on one of its components being extreme.

Let $Y(\mathbf{s})$ be a random process defined over space ($\mathbf{s} \in \mathcal{S} \subset \mathbb{R}^2$) with Laplace margins. For this random process, Wadsworth and Tawn (2022) assume the existence of standardising functions $a(\mathbf{s}; \mathbf{s}_0, y_0)$ and $b(\mathbf{s}; \mathbf{s}_0, y_0)$ such that, for a large enough threshold t ,

$$[Y(\mathbf{s}) \mid Y(\mathbf{s}_0) = y_0 > t] \stackrel{d}{=} a(\mathbf{s}; \mathbf{s}_0, y_0) + b(\mathbf{s}; \mathbf{s}_0, y_0)Z(\mathbf{s}; \mathbf{s}_0), \quad \mathbf{s}, \mathbf{s}_0 \in \mathcal{S}, \quad (7)$$

where $Z(\mathbf{s}; \mathbf{s}_0)$ is a random process satisfying $Z(\mathbf{s}_0; \mathbf{s}_0) = 0$ almost surely, and $a(\mathbf{s}; \mathbf{s}_0, y_0) \leq y_0$, with equality when $\mathbf{s} = \mathbf{s}_0$. It can be shown that $Y(\mathbf{s})$ and $Y(\mathbf{s}_0)$ are extremally dependent when $a(\mathbf{s}; \mathbf{s}_0, y_0) = y_0$ and $b(\mathbf{s}; \mathbf{s}_0, y_0) = 1$, while they are extremally independent when $a(\mathbf{s}; \mathbf{s}_0, y_0) < y_0$, with larger values of $a(\cdot)$ and $b(\cdot)$ corresponding to larger degrees of subasymptotic dependence (Heffernan & Tawn, 2004). Wadsworth and Tawn (2022) provides some guidance on parametric functions for $a(\cdot)$ and $b(\cdot)$ together with parametric distributions for $Z(\cdot)$ that cover a large range of already existing models. To perform inference with high-dimensional models, they further propose to model $Z(\cdot)$ as a random process with a Gaussian copula and delta-Laplace marginal distributions. Their proposed model for $Z(\cdot)$ has later seen usage by Shooter et al. (2021) and Richards et al. (2022).

In order to perform Bayesian inference for the spatial conditional extremes model with R-INLA, E. S. Simpson et al. (2020) cast (7) into the latent Gaussian modelling framework by adding a Gaussian nugget effect and requiring $Z(\cdot)$ to be a Gaussian random field. This gives the model

$$[Y(\mathbf{s}) \mid Y(\mathbf{s}_0) = y_0 > t] \stackrel{d}{=} a(\mathbf{s}; \mathbf{s}_0, y_0) + b(\mathbf{s}; \mathbf{s}_0, y_0)Z(\mathbf{s}; \mathbf{s}_0) + \epsilon(\mathbf{s}; \mathbf{s}_0), \quad (8)$$

where $\epsilon(\mathbf{s}; \mathbf{s}_0)$ is Gaussian white noise with constant precision, satisfying $\epsilon(\mathbf{s}_0; \mathbf{s}_0) = 0$ almost surely. To further speed up inference, they also assume that $Z(\cdot)$ has zero mean and a Matérn covariance structure, so that it can be approximated by a sparse Gaussian Markov random field using the SPDE approach of Lindgren et al. (2011). Based on the guidelines of Wadsworth and Tawn (2022), they choose $b(\mathbf{s}; \mathbf{s}_0, y_0) = y_0^\beta$ with $0 \leq \beta < 1$, whereas for $a(\cdot)$ they propose the semiparametric spline model

$$a(\mathbf{s}; \mathbf{s}_0, y_0) = \alpha(\|\mathbf{s} - \mathbf{s}_0\|)y_0 + \gamma(\|\mathbf{s} - \mathbf{s}_0\|),$$

where $\alpha(\cdot)$ and $\gamma(\cdot)$ are spline functions with $\alpha(0) = 1$ and $\gamma(0) = 0$.

Here, we adopt the model in (S1.1) and keep the somewhat strict requirement of modelling $Z(\cdot)$ as a Gaussian random field using the SPDE approximation. However, we propose some important modifications that allow for faster inference and more flexible model building:

- Using the recent **cgeneric** framework, which allows us to implement model components that are not readily available in R-INLA using the C programming language, we propose a general method for implementing the model (S1.1) in R-INLA such that $a(\cdot)$ and $b(\cdot)$ can take any kind of form, both parametric and semiparametric.
- We explain why it is problematic to constrain $Z(\mathbf{s}; \mathbf{s}_0)$ as in Wadsworth and Tawn (2022) and E. S. Simpson et al. (2020), and demonstrate an efficient constraining method that gives better properties for $Z(\mathbf{s}; \mathbf{s}_0)$.

Both of these modifications are described in Section S1 in the supplementary materials.

3.2 Inference

Inference for the conditional extremes model can be performed by choosing one conditioning site $\mathbf{s}_0 \in \mathcal{S}$ and a large threshold t . The parameters of the standardising functions $a(\cdot)$ and $b(\cdot)$, the residual field $Z(\cdot)$ and the nugget effect $\epsilon(\cdot)$ can then be estimated using all observations where $Y(\mathbf{s}_0) > t$. Since this approach only allows us to use observations from times when $Y(\mathbf{s}_0)$ is extreme, it yields separate model fits for each conditioning site in \mathcal{S} . Under stationarity, it is reasonable to believe that inference could be strengthened by combining information from multiple conditioning sites into one global model fit. If we assume a stationary model, in the sense that the parameters of $a(\cdot)$, $b(\cdot)$, $Z(\cdot)$ and $\epsilon(\cdot)$ are independent of the choice of \mathbf{s}_0 , a global model fit can be achieved by performing inference with the composite likelihood of Heffernan and Tawn (2004) and Wadsworth and Tawn (2022). Given observations $\mathcal{Y} = \{y_j(\mathbf{s}_i) : j = 1, 2, \dots, n, i = 1, 2, \dots, d\}$ of the random process at n time points and d locations, the composite log-likelihood may be expressed as

$$\ell_c(\boldsymbol{\theta}; \mathcal{Y}) = \sum_{i=1}^d \sum_{j=1}^n \ell(\boldsymbol{\theta}; \mathbf{y}_j \mid y_j(\mathbf{s}_i)) I(y_j(\mathbf{s}_i) > t). \quad (9)$$

Here, $\ell(\cdot)$ is the log-likelihood of the conditional extremes model in (S1.1), \mathbf{y}_j is a d -dimensional vector containing all observations from time point j , $I(\cdot)$ is an indicator function and $\boldsymbol{\theta}$ contains all the parameters of $a(\cdot)$, $b(\cdot)$, $Z(\cdot)$ and $\epsilon(\cdot)$.

As described in Section 2, the downside of performing Bayesian inference with a composite likelihood is that the resulting posterior distribution might have poor frequency properties and become too focused or too wide. To the best of our knowledge, our paper is the first attempt to perform Bayesian inference for the spatial conditional extremes model based on the composite likelihood in (9).

4 Simulation studies

We evaluate the performance of our adjustment method through several simulation studies, considering different composite and/or misspecified likelihoods described in Section 1. In Section 4.1, a Gaussian distribution is fitted to univariate data from a Student's t -distribution. In Section 4.2, an SPDE approximation of low rank is applied for modelling data from a spatial Gaussian random field. In Section 4.3, inference on a spatial Gaussian random field is performed using a block composite likelihood. Finally, in Section 4.4, the composite likelihood approach for the spatial conditional extremes model is considered. In each study we adjust the posteriors and compare frequency properties between the unadjusted and the adjusted credible intervals.

Table 1: Coverage percentage for the unadjusted and adjusted credible intervals for three different credible interval sizes.

Aim	Unadjusted	Adjusted
90%	11%	94%
95%	13%	98%
99%	15%	100%

4.1 Univariate misspecified model

We here simulate data from a Student’s t -distribution with one degree of freedom and estimate their median $\theta = 0$ using a Gaussian distribution with a fixed variance of 1. Since both the Student’s t -distribution and the Gaussian distribution are symmetric, the KLD minimiser between the true Student’s t -distribution and the misspecified Gaussian distribution is $\theta^* = \theta = 0$. However, due to the heavy tails of the Student’s t -distribution and the small, fixed variance of the Gaussian model, the posterior for θ will often be too focused. Thus, credible intervals will be too thin, meaning that an estimated $(1 - \alpha)$ -credible interval will contain θ^* considerably less often than $(1 - \alpha) \times 100\%$ of the times, which should be the correct asymptotic coverage probability when the effect of the prior is negligible. A correct adjustment will therefore increase the variance of the posterior distribution and create wider credible intervals.

To check this, we sample 100 observations from the Student’s t -distribution and choose a Gaussian prior for θ with mean 0 and precision 0.001. Adjusted and unadjusted credible intervals are then created using R-INLA and the adjustment method from Section 2.2. This is repeated 1000 times. Coverage probabilities are then estimated by counting how many of the 1000 credible intervals include θ^* . Results are displayed in Table 1. As expected, the unadjusted credible intervals are considerably too thin, with, e.g., the 95% intervals containing θ^* in only 13% of the experiments, whereas the adjusted coverage percentage is 98%. Similar improvements are found for the 90% and 99% credible intervals. In practice, one would of course never fix the variance to 1 when fitting a Gaussian distribution in this context. However, this toy example serves as a simple demonstration for how misspecified models can result in credible intervals with poor frequency properties, and how these can be greatly improved by simply adjusting the posterior, using our proposed method.

4.2 Low-rank SPDE approximation

We now simulate data from a Gaussian random field $Z(\mathbf{s})$ with Matérn covariance function

$$\text{Cov}(Z(\mathbf{s}), Z(\mathbf{s}')) = \frac{\sigma^2}{2^{\nu-1}\Gamma(\nu)} (\kappa \|\mathbf{s} - \mathbf{s}'\|)^\nu K_\nu(\kappa \|\mathbf{s} - \mathbf{s}'\|),$$

with variance σ^2 , range $\rho = \sqrt{8\nu}/\kappa > 0$ for some $\kappa > 0$, and known smoothness parameter $\nu > 0$. Here, K_ν is the modified Bessel function of the second kind and order ν . We also add

Table 2: Coverage percentages for unadjusted and adjusted credible intervals using the SPDE approach with a too coarse mesh.

Aim	τ	τ_{adj}	ρ	ρ_{adj}	σ	σ_{adj}
90%	48%	93%	91%	90%	90%	90%
95%	55%	97%	95%	95%	95%	96%
99%	69%	99%	99%	98%	100%	99%

a Gaussian nugget effect with precision τ . Parameter estimation is then performed using an SPDE approximation of low rank, i.e., based on a coarse mesh used to discretise the spatial domain. Such low-rank approximations are typically unable to capture all the variability in the data, which means that the nugget effect has to explain a large percentage of the variance, leading to underestimation of the precision τ . Thus, we expect the KLD minimiser $\boldsymbol{\theta}^*$ to be different from the true parameters $\boldsymbol{\theta} = (\tau, \rho, \sigma)^T$.

We sample 200 replicates of the spatial field on the domain $\mathcal{S} = [0, 25] \times [0, 25]$ and observe it at 400 random locations. True parameters are set to $\boldsymbol{\theta} = (\tau, \rho, \sigma)^T = (100, 12, 1)^T$ with smoothness $\nu = 1.5$. We assign τ a gamma prior with shape 1 and scale 2×10^4 , while ρ and σ are given a joint penalised complexity (PC) prior (Fuglstad et al., 2019; D. Simpson et al., 2017), setting $P(\rho < 12) = 0.5$ and $P(\sigma > 1) = 0.5$. We compute both unadjusted and adjusted credible intervals for the three parameters. This is repeated 300 times, using the same locations, but new observations each time.

To estimate the unknown KLD minimiser $\boldsymbol{\theta}^*$, we simulate 10^4 replications of the Gaussian Matérn field and compute the maximum likelihood estimator for the misspecified SPDE model. This gives $\boldsymbol{\theta}^* = (\tau^*, \rho^*, \sigma^*) \approx (13.0, 14.5, 1.2)^T$. As expected, τ is severely underestimated, while ρ and σ are slightly overestimated.

Table 2 displays estimated coverage probabilities detailing how often the parameters of $\boldsymbol{\theta}^*$ are included in their respective credible intervals. The adjustment of the posterior yields a considerable improvement for τ . The unadjusted frequency properties of ρ and σ , however, are already good, and our adjustment method does not deteriorate the credible intervals for these parameters.

4.3 Block composite spatial Gaussian likelihood

In this other experiment, we test how the adjustment method works with a block composite likelihood (Eidsvik et al., 2014). To do so we sample 100 realisations from a Gaussian Matérn field with parameters and domain as in Section 4.2. This time we generate samples directly using the SPDE approximation, so no model misspecification is introduced when using it for inference. As in Section 4.2 we observe the fields at 400 random locations.

Inference is performed using a block composite likelihood, whereby the spatial domain is divided into 25 disjoint blocks of size 5×5 , all wrongly assumed to be independent of each other. This is in some sense a milder misspecification than in Section 4.2, as it gives

Table 3: Coverage percentages for unadjusted and adjusted credible intervals using the block composite likelihood.

Aim	τ	τ_{adj}	ρ	ρ_{adj}	σ	σ_{adj}
90%	88%	89%	61%	90%	61%	91%
95%	96%	94%	71%	93%	67%	96%
99%	99%	100%	83%	99%	77%	99%

$\theta^* = \theta$. On the other hand, such independence assumptions typically lead to overconfidence in the posterior, meaning that credible intervals will become too thin. A correct adjustment is therefore expected to increase the variance of the posterior. Unadjusted and adjusted credible intervals are created using **R-INLA** with the SPDE approach, where the priors for $\theta = (\rho, \sigma^2, \tau)$ are the same as in Section 4.2. The experiment is repeated 300 times.

Table 3 displays estimated coverage probabilities for the model parameters. As expected, the unadjusted credible intervals are often too thin, and the adjustment method successfully increases the posterior variance to provide improved coverage probabilities.

4.4 Spatial conditional extremes model

We evaluate our adjustment method when applied to the spatial conditional extremes model (S1.1) with a global model fit based on the composite likelihood in (9). In the simulation experiment we replicate the setup of the case study in Section 5. The standardising functions $a(\cdot)$ and $b(\cdot)$ are defined as

$$a(\mathbf{s}; \mathbf{s}_0, y_0) = y_0 \exp \{-(d/\lambda)^\kappa\}, \quad b(\mathbf{s}; \mathbf{s}_0, y_0) = \sigma \sqrt{1 - \exp(-2d/\rho_b)}, \quad (10)$$

with $d = \|\mathbf{s} - \mathbf{s}_0\|$ and parameters $(\lambda, \kappa, \sigma, \rho_b)$, all strictly positive. Furthermore, the threshold t is set equal to the 99.75% quantile of the Laplace distribution. The residual field, $Z(\cdot)$, is an SPDE approximation to a Gaussian Matérn field with a fixed variance of 1 and range parameter ρ , created using the mesh seen in the left subplot of Figure 1. Note that, since $b(\mathbf{s}_0; \mathbf{s}_0, y_0) = 0$, we do not need to enforce that $Z(\mathbf{s}_0; \mathbf{s}_0) = 0$. The nugget effect $\epsilon(\cdot)$ is defined as Gaussian white noise with zero mean and precision τ . In order to produce realisations that mimic the real data application, parameter values are set to $\theta = (\lambda, \kappa, \sigma, \rho_b, \rho, \tau)^T \approx (19.1, 0.6, 1.9, 4.6, 13.0, 23.1)^T$, where λ , ρ_b and ρ have unit km. Priors for θ are displayed in Table 4. See Section 5 for more details and explanations.

To ensure that our model implementation works as it should we first choose one location $\mathbf{s}_0 \in \mathcal{S}$ and simulate from the conditional extremes model using \mathbf{s}_0 as conditioning site. Parameters are then recovered from the data using our implemented model in **R-INLA**. We find that the implemented methodology accurately estimates the parameters. However, we also find that **R-INLA** struggles considerably when initial values are too far away from θ . Consequently, we choose to divide inference into two steps: First we compute the maximum likelihood estimator using the **R** function `optim()`. Then we use the maximum likelihood

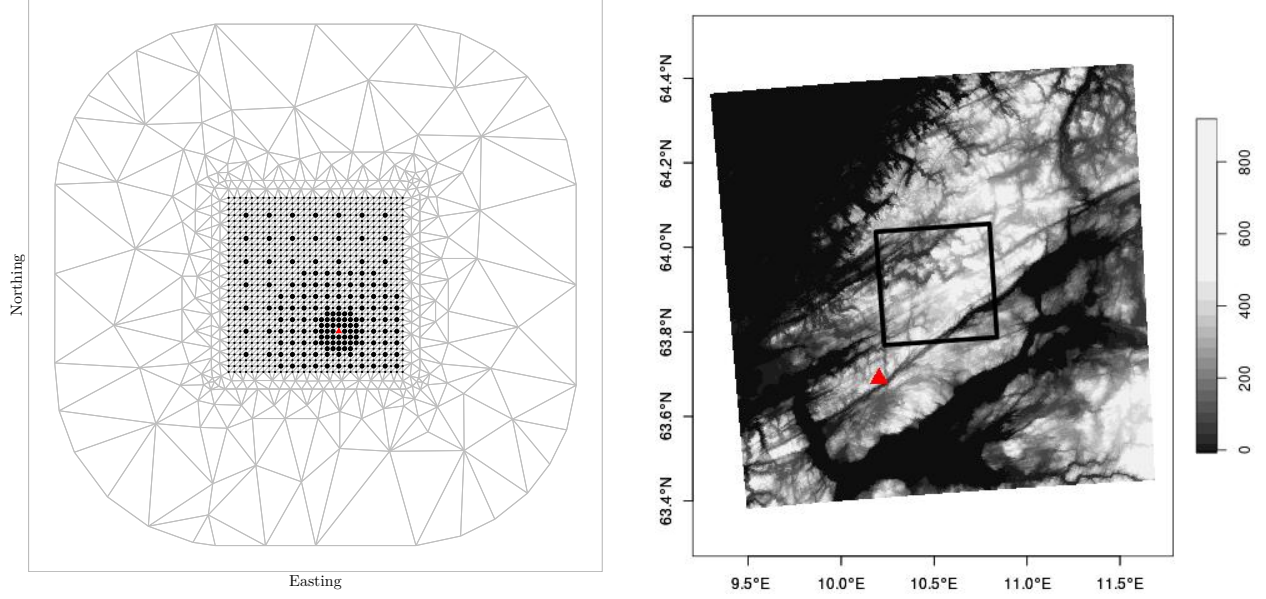


Figure 1: Left plot: Given a conditioning site s_0 (displayed with (▲)), locations used for inference are displayed as big black dots (●) and locations in \mathcal{S} that are not used for inference are displayed as small black dots (·). The SPDE mesh is displayed in grey. Right plot: Elevation (m) map, over the Fosen area in central Norway. The study area \mathcal{S} is located inside the black rectangle, and the Rissa radar is displayed using a triangle (▲).

Table 4: Prior distributions of the conditional extremes parameters. $\mathcal{N}(\mu, \sigma^2)$ denotes the Gaussian distribution with mean μ and variance σ^2 . $\Gamma(a, b)$ denotes the gamma distribution with shape parameter a and scale parameter b . The parameters ρ and σ are given the joint PC prior of Fuglstad et al. (2019) such that $P(\rho < 60) = 0.95$ and $P(\sigma > 4) = 0.05$.

$\log(\lambda) \sim \mathcal{N}(4, 3^2),$	$\log(\rho_b) \sim \mathcal{N}(\log(6), 2^2),$	$\rho \sim \text{PC}(60, 0.95),$
$\log(\kappa) \sim \mathcal{N}(-0.4, 3^2),$	$\tau \sim \Gamma(1, 2 \cdot 10^4),$	$\sigma \sim \text{PC}(4, 0.05),$

Table 5: Coverage percentages for unadjusted and adjusted credible intervals based on the composite spatial conditional extremes likelihood.

Aim	λ	λ_{adj}	κ	κ_{adj}	σ	σ_{adj}	ρ_b	$\rho_{b\text{adj}}$	ρ	ρ_{adj}	τ	τ_{adj}
90%	27%	69%	54%	72%	32%	71%	78%	83%	36%	71%	66%	84%
95%	33%	75%	63%	80%	40%	79%	85%	87%	40%	76%	76%	90%
99%	43%	84%	78%	88%	49%	85%	92%	93%	54%	87%	87%	96%

estimator as initial values for R-INLA. This requires approximately the same amount of computational resources, but yields considerably better results, than simply using R-INLA without first computing the maximum likelihood estimator.

For evaluating the adjustment method, we sample from the distribution of

$$\left[\{Y(\mathbf{s}) : \mathbf{s} \in \mathcal{S}\} \mid \max_{\mathbf{s} \in \mathcal{S}} Y(\mathbf{s}) > t \right], \quad (11)$$

defined such that the spatial conditional extremes model holds for each conditioning site $\mathbf{s} \in \mathcal{S}$. Different simulation algorithms for sampling from this distribution have been developed by Keef, Tawn, et al. (2013) and Wadsworth and Tawn (2022). We use the method of Wadsworth and Tawn (2022) as we find it to be more efficient for high-dimensional spatial models where $a(\cdot)$ does not decay quickly to zero and $b(\cdot)$ is of the same magnitude as the threshold t . A considerable problem with the distribution of (11), described by Heffernan and Tawn (2004) and Liu and Tawn (2014), is that it lacks self-consistency, i.e., it is not consistent with the individual models based on single conditioning sites (see Appendix A for a more detailed explanation). In short, the consequence of this self-inconsistency is that $\boldsymbol{\theta}^* \neq \boldsymbol{\theta}$ even when we fit the distribution of (11) to data sampled from the distribution of (11) with parameters $\boldsymbol{\theta}$. Thus, we must estimate $\boldsymbol{\theta}^*$ before we can evaluate frequency properties. To estimate $\boldsymbol{\theta}^*$, we sample 5×10^4 replications of (11) and compute the maximum composite likelihood estimator using (9). This gives $\hat{\boldsymbol{\theta}}^* \approx (15.5, 0.8, 1.9, 1.5, 13.1, 20.1)^T \neq \boldsymbol{\theta}$.

Finally, we evaluate the adjustment method in a similar fashion as the previous simulation studies. We sample 10 replications from the distribution of (11) and fit the composite conditional extremes model to all observed threshold exceedances. For the chosen design, 10 replications from the distribution of (11) correspond to between 100 and 200 threshold exceedances over all the chosen conditioning sites. The simulation experiment is repeated 300 times. Coverage percentages for the unadjusted and adjusted posteriors are displayed in Table 5. Once again, the adjusted posterior has considerably better frequency properties than the unadjusted posterior, though, the adjusted posterior properties are not as good as in the previous simulation studies. As demonstrated in Section S2 in the supplementary material, this is most likely caused by the complications of simulating from a self-inconsistent distribution. There, we perform a similar experiment where the global spatial conditional extremes model is fitted to extremes from a spatial Gaussian random process, and the adjusted posteriors once again perform as well as in the three previous simulation studies.

5 Case study: Extreme precipitation in Norway

We apply our proposed methodology to the modelling of extreme hourly precipitation in Norway. Data are presented in Section 5.1 and the inference is described in Section 5.2. Results are presented and evaluated in Section 5.3.

5.1 Data

We consider $1 \times 1 \text{ km}^2$ maps of mean hourly precipitation, produced by the Norwegian Meteorological Institute by processing raw reflectivity data from the weather radar located in Rissa ($63^\circ 41' 26''\text{N}$, $10^\circ 12' 14''\text{E}$) in central Norway. Such maps are available online (<https://thredds.met.no>), dating back to 1 January 2010. We extract data from a rectangular domain, close to the Rissa radar, of size $31 \times 31 \text{ km}^2$. Denote the set of all grid points in the rectangular domain as \mathcal{S} . We then have $|\mathcal{S}| = 961$ unique locations containing hourly precipitation estimates. A map containing \mathcal{S} and the Rissa radar is displayed in the right subplot of Figure 1. For each $\mathbf{s} \in \mathcal{S}$, we extract all hourly observations from the summer months (June, July and August) for the years 2010–2021. Removal of missing data gives a total of 25512 observations at each location.

5.2 Modelling and inference

To fit the conditional extremes model to precipitation data, we must first standardise the data to have Laplace marginals and choose parametric forms for the functions $a(\cdot)$ and $b(\cdot)$. This is described in Section S3 in the supplementary material, where we choose the parametric forms displayed in (10). Furthermore, the threshold t is set equal to the 99.75% quantile of the Laplace distribution, and the residual field $Z(\cdot)$ is assumed to have a fixed variance of 1 and range parameter ρ . Bayesian inference with the spatial conditional extremes model is performed using the composite likelihood in (9). Using all locations in \mathcal{S} as conditioning sites is computationally demanding, so we define a regular sub-grid of resolution $4 \times 4 \text{ km}^2$ and use all locations on the sub-grid as conditioning sites. This yields a total of 49 conditioning sites, each containing between 15 to 42 available threshold exceedances. The posterior adjustment method is then applied to the output of R-INLA for improving its frequency properties. In order to compare the global model to models based on only one conditioning site, we also create ten single site model fits, based on ten different conditioning sites. The first conditioning site is chosen as the location on the $4 \times 4 \text{ km}^2$ resolution sub-grid that contains the most threshold exceedances, while the remaining nine locations are randomly selected in \mathcal{S} . The single site model fits are all based on valid likelihoods, but they might still be misspecified, e.g., since the choice of modelling the residual field as a Gaussian SPDE approximation was made solely for computational reasons, meaning that it does not necessarily provide a perfect fit to the actual precipitation data. Therefore, the posterior adjustment method is also applied to all ten single site fits.

The preliminary study in Section S3 of the supplementary material shows that the largest changes in $a(\cdot)$ and $b(\cdot)$ occur close to \mathbf{s}_0 . However, most of the locations in \mathcal{S} are far away from \mathbf{s}_0 , where there is less information to be gained. To account for this and give more weight to close-by locations, we discard some of the observations far away from \mathbf{s}_0 during inference, which also speeds up inference. The left subplot of Figure 1 shows an example of the locations used to perform inference for 1 of the 49 chosen conditioning sites of the global model fit. Similar patterns are used for all other conditioning sites, and also for the single site model fits.

Using the SPDE approach to model $Z(\cdot)$ requires that we define a triangular mesh. The mesh needs to be very fine in order to capture the rapid changes in $b(\cdot)$ close to \mathbf{s}_0 (see Section S1 of the supplementary material for a detailed discussion). Consequently, our mesh has a node at each $\mathbf{s} \in \mathcal{S}$, allowing us to accurately capture the changes in $b(\cdot)$ at every location on the grid. The mesh used for all conditioning sites is displayed in Figure 1.

Priors for all model parameters (λ, κ, σ and ρ_b from (10), the range ρ in $Z(\mathbf{s}; \mathbf{s}_0)$ and τ in $\epsilon(\mathbf{s}; \mathbf{s}_0)$) are described in Table 4. All priors are relatively informative to avoid unrealistic behaviour, but have large enough variance to ensure that they are not overly informative.

The posterior adjustment method is applied to the global and all the single site model fits. As described in Section 2.2, estimates for $\boldsymbol{\theta}^*$ and $\mathbf{H}(\boldsymbol{\theta}^*)$ are provided directly from R-INLA, while $\mathbf{J}(\boldsymbol{\theta}^*)$ is estimated by computing gradients of the log-likelihood, using numerical derivation, and then computing the expression in (5), using a sliding window approach with a window radius of 5 hours. For each posterior distribution, $\boldsymbol{\theta}^*$, $\mathbf{H}(\boldsymbol{\theta}^*)$ and $\mathbf{J}(\boldsymbol{\theta}^*)$ are estimated using only the data that were available during inference, meaning that different estimates are computed for each model fit, and the estimates for the global model are based on more data than the estimates for the single site models.

5.3 Results

We fit the global and the ten single site models to data. Posteriors are displayed in Figure 2. For better visibility, not all posterior distributions are represented, but those displayed are representative of the patterns observed. The posterior from the unadjusted global model is considerably more focused than all other posterior distributions for most parameters, whereas the adjusted global posterior has a more reasonable width. Interestingly, the opposite holds for ρ_b , where the unadjusted global posterior is wider than all other posteriors, and the adjusted global posterior is the most focused. The adjusted single site posteriors are somewhat similar to the unadjusted single site posteriors for κ and ρ_b , and considerably wider than the unadjusted posteriors for all other parameters. There is also much variability between the single site model fits, and the global posteriors are mainly located somewhere in the middle of all the single site posteriors.

The estimated values of ρ_b are very small, yielding an estimated function $b(\cdot)$ that is approximately constant for all $\mathbf{s} \neq \mathbf{s}_0$. We also examine the posteriors of $a(\mathbf{s}; \mathbf{s}_0, \cdot)$ and $b(\mathbf{s}; \mathbf{s}_0, \cdot)$ for different distances $d = \|\mathbf{s} - \mathbf{s}_0\|$, and find similar patterns as those in Figure 2:

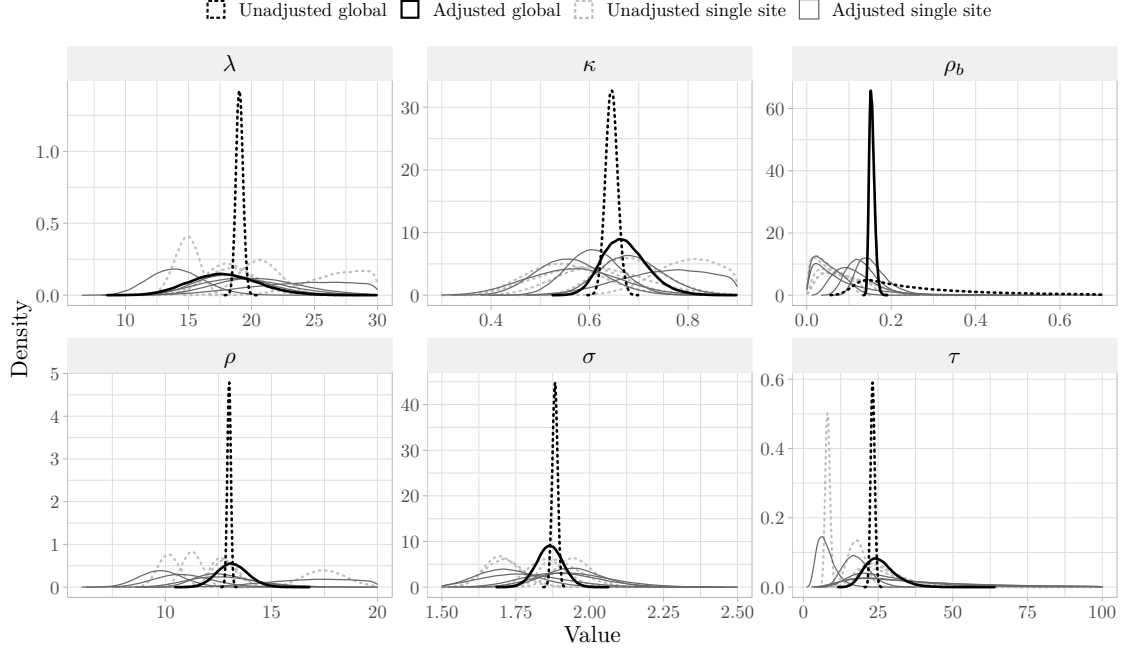


Figure 2: Posterior distributions for a subset of the fitted models. The displayed single site posteriors correspond to single site models nr. 2, 3, 7, 8 and 9.

there is considerable variability between the single site posteriors, and the global posteriors are located approximately in the middle of the single site posteriors (results not shown).

We then perform model evaluation using the log-score (e.g., Gneiting & Raftery, 2007). For each of the model fits, marginal likelihoods are estimated using Monte Carlo estimation, i.e., given n_s samples $\theta_1, \dots, \theta_{n_s}$ from the posterior of model \mathcal{M} , the marginal likelihood is estimated as

$$\hat{L}(\mathcal{M}; \mathcal{Y}) = \frac{1}{n_s} \sum_{i=1}^{n_s} L_{\mathcal{M}}(\theta_i; \mathcal{Y}),$$

where $L_{\mathcal{M}}$ is the likelihood of model \mathcal{M} . The estimated log-score $\hat{\ell}(\mathcal{M}; \mathcal{Y})$ is then the logarithm of $\hat{L}(\mathcal{M}; \mathcal{Y})$. For two competing models, \mathcal{M}_1 and \mathcal{M}_2 , we conclude that \mathcal{M}_1 provides a better fit to data \mathcal{Y} if $\hat{\ell}(\mathcal{M}_1; \mathcal{Y}) > \hat{\ell}(\mathcal{M}_2; \mathcal{Y})$.

In order to evaluate out-of-sample performance, log-scores are estimated using threshold exceedances from all the 912 conditioning sites in \mathcal{S} that were not used for fitting the global model. To the best of our knowledge, the theory behind the log-score is based on valid likelihoods, but the conditional extremes composite likelihood is not a valid likelihood function. Thus, we choose not to directly compare global log-scores based on the entire test set. Instead, for each of the 912 conditioning sites, we estimate the marginal likelihood of each model using only threshold exceedances from that single site. Log-scores are then separately compared and ranked for each conditioning site. We estimate the log-scores using $n_s = 500$ samples.

Figure 3 displays histograms of the 912 rankings of all the model fits. The posterior

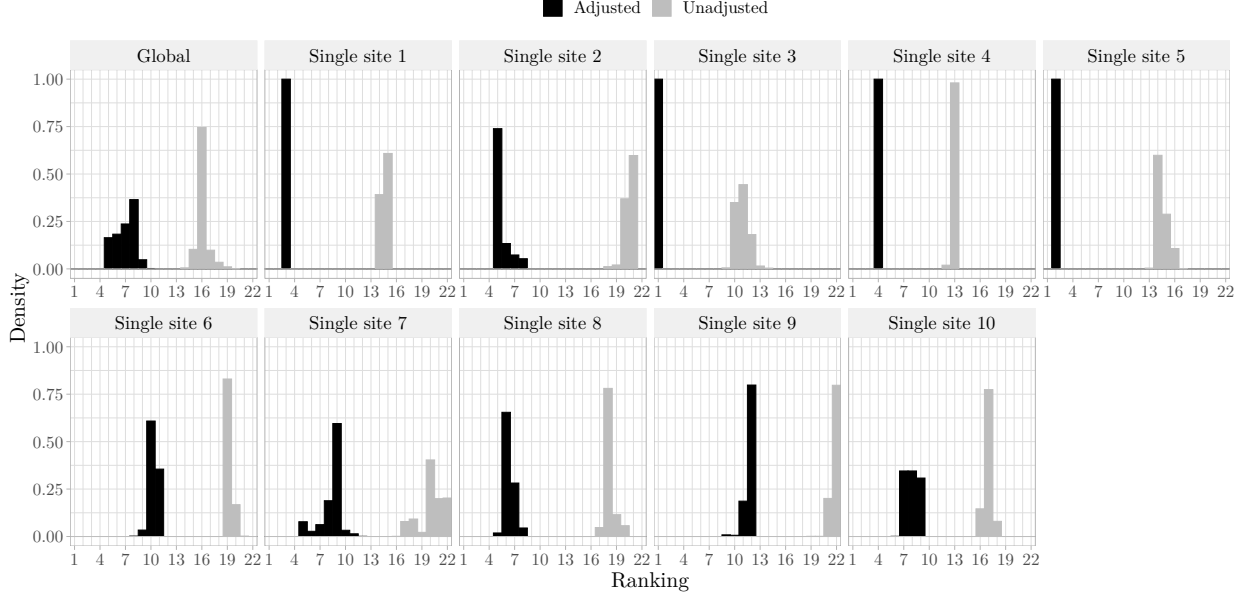


Figure 3: Histograms displaying the log-score rankings of all 22 model fits, at 912 different conditioning sites, where 1 is best and 22 is worst. Unadjusted model fits are displayed in grey, while adjusted ones are displayed in black.

adjustment method improves the log-score of every single model, not just for the global model based on a composite likelihood. This once again demonstrates the effectiveness of the posterior adjustment method. Through its usage we have both learned that there is considerable misspecification present in all original model fits, and we have been able to improve them by accounting for this misspecification.

Figure 3 also shows that the global model fit is outperformed by approximately half of the single site model fits, even though the global model fit is based on approximately 50 times more data. This suggests that the distribution of the precipitation data is not stationary in the sense that $a(\cdot)$, $b(\cdot)$, $Z(\cdot)$ and $\epsilon(\cdot)$ only depend on the distance $\|\mathbf{s} - \mathbf{s}_0\|$ between \mathbf{s} and the conditioning site \mathbf{s}_0 . The value of the KLD minimiser $\boldsymbol{\theta}^*$ for the global model is therefore the value that on average provides a best fit to data from the 49 conditioning sites used for inference. However, this average is not guaranteed to be close to the best fit for any one of the conditioning sites. The adjustment method generally widens the global posterior to improve its frequency properties, but this is different from changing the meaning of the posterior from “what it is” to “what we want it to be” (Walker, 2013). Note that the global model might, however, still be useful for the given data set. If, e.g., the threshold t was chosen so large that less than two exceedances were available at each conditioning site, inference would be impossible for the single site models, while the global model would still provide useful results.

6 Conclusion

A novel adjustment method is proposed for improving the frequency properties of posterior distributions that are based on composite and/or misspecified likelihoods. The method performs the required adjustment through postprocessing, which makes it able to work in conjunction with a large variety of efficient inference programs for Bayesian inference, such as R-INLA. Several simulation studies are performed, and they all show considerable improvements in model fit after applying the adjustment method. The adjustment method is further applied to high-dimensional Bayesian modelling of precipitation extremes with the spatial conditional extremes model, using both single site likelihoods and a global composite likelihood. An improved implementation of the spatial conditional extremes model in R-INLA is also developed. The results once again show that the adjustment method performs satisfactorily, with all adjusted model fits outperforming their unadjusted counterparts. The global model fit is outperformed by several single site model fits. This indicates that the distribution of extreme precipitation might be nonstationary over the study domain.

Our simulation studies and the real data application show that the adjustment method consistently improves model fits for Bayesian models based on composite and/or misspecified likelihoods, without deteriorating the performance of models that already have good frequency properties. Since all models for natural phenomena are misspecified to a certain degree, the adjustment method may allow for a simple way of improving model fits in a large variety of settings, including spatial, temporal and spatio-temporal applications.

A Self-inconsistency of the conditional extremes model

As discussed by Besag (1974), if one defines a joint distribution by specifying a set of conditional distributions, the resulting joint distribution may become self-inconsistent. This means that joint probabilities may not be well defined, because different ways of integrating over the conditional distributions can yield different answers. Since the conditional extremes distribution is defined through a set of conditional distributions, its joint distribution may therefore become self-inconsistent. This self-inconsistency is examined by Heffernan and Tawn (2004) and Liu and Tawn (2014), who show that it is impossible to achieve self-consistency for finite thresholds t , given extremal independence, i.e., $a(\mathbf{s}; \mathbf{s}_0, y_0) < y_0$, when the distribution of the residual field $Z(\cdot)$ is smooth. The consequence of this self-inconsistency is that probabilities for events where more than one random variable is extreme are ill-defined. As an example, assume that the bivariate vector $(X, Y)^T$ can be described by the conditional extremes model with threshold t . The probability $P(X > t, Y > t)$ that both components exceed the threshold can, e.g., be computed as

$$\int_t^\infty \int_t^\infty \pi(x | y) \pi(y) dy dx, \quad \text{or} \quad \int_t^\infty \int_t^\infty \pi(y | x) \pi(x) dx dy,$$

where $\pi(\cdot)$ denotes different kinds of probability density functions. Due to the lack of self-consistency between conditional models for $\pi(x | y)$ and $\pi(y | x)$, these two integration paths might provide different answers.

The lack of self-consistency causes problems when one attempts to simulate from the global conditional extremes distribution (11), which in the bivariate case is the joint distribution of $[(X, Y) | \max(X, Y) > t]$. In order to sample from this distribution, one must first choose one specific integration path and define it as the “correct one”. Then, one must sample in a way that corresponds to this integration path. Consequently, two different simulation algorithms for the global conditional extremes distribution may produce samples with considerably different properties. As an example, for a d -dimensional random vector \mathbf{X} , the simulation algorithm of Keef, Tawn, et al. (2013) is based on estimating probabilities as

$$P(\mathbf{X} \in \cdot | \max(\mathbf{X}) > t) = \sum_{i=1}^d \pi_i^{(1)} \frac{P(\mathbf{X} \in \cdot, X_i = \max(\mathbf{X}) | X_i > t)}{P(X_i = \max(\mathbf{X}) | X_i > t)}, \quad (\text{A.1})$$

where $\pi_i^{(1)} = P(X_i = \max(\mathbf{X}) | \max(\mathbf{X}) > t)$, while the Wadsworth and Tawn (2022) algorithm is based on estimating probabilities as

$$P(\mathbf{X} \in \cdot | \max(\mathbf{X}) > t) = \frac{\sum_K \sum_{i=1}^d \pi_i^{(2)} P(\mathbf{X} \in \cdot \cap R_K | X_i > t) / |K|}{\sum_K \sum_{i=1}^d \pi_i^{(2)} P(\mathbf{X} \in R_K | X_i > t) / |K|}, \quad (\text{A.2})$$

where $\pi_i^{(2)} = P(X_i > t) / \sum_{j=1}^d P(X_j > t)$, K is an element in the power set of $\{1, 2, \dots, d\}$, and

$$R_K = \{\mathbf{x} = (x_1, \dots, x_d)^T \in \mathbb{R}^d : x_i > t \forall i \in K, x_j \leq t \forall j \notin K\}.$$

These two algorithms clearly correspond to two different integration paths, and may therefore provide different results, when combined with different conditional extremes models.

We compute $P(X > t, Y > t | \max(X, Y) > t)$ using the two integration paths (A.1) and (A.2), for the symmetrical conditional extremes model where X and Y have exponential marginals and the conditional distribution of $[X | Y > t]$ is Gaussian with mean $\mu + \alpha Y$ and variance $\sigma^2 Y^{2\beta}$, and vice versa for $[Y | X > t]$. If $\mu = 0$, $\sigma = 1$, $\alpha = 0.9$, $\beta = 0.8$ and $t = 4$, then equation (A.1) gives a probability of 0.17, whereas equation (A.2) gives a probability of 0.37. We also estimate the probability using Monte Carlo simulation and find, as expected, that the Keef, Tawn, et al. (2013) algorithm agrees with (A.1), while the Wadsworth and Tawn (2022) algorithm agrees with (A.2). This massive difference in computed probabilities could potentially have severe consequences for, e.g., infrastructure built to withstand a certain return level of hourly precipitation. As none of the possible integration paths are neither more nor less correct than the others, it is our opinion that one should be extremely careful when estimating return levels by sampling from the conditional extremes model where the conditioning variable is unknown, i.e., $[\mathbf{X} | \max(\mathbf{X}) > t]$. Instead, we believe that one should prefer to estimate return levels by first choosing a specific conditioning site/variable, e.g., X_i , and then sampling from the conditional extremes distribution of $[\mathbf{X} | X_i > t]$, which is both proper and self-consistent.

Acknowledgements

The authors are grateful to Jordan Richards and Håvard Rue for many helpful discussions.

Funding Raphaël Huser was partially supported by the King Abdullah University of Science and Technology (KAUST) Office of Sponsored Research (OSR) under Award No. OSR-CRG2020-4394.

Conflict of interest The authors report there are no competing interests to declare.

Code and data availability The necessary code and data for achieving these results are available online at <https://github.com/siliusmv/posteriorAdjustment>.

References

- Banerjee, S., Carlin, B. P., & Gelfand, A. E. (2014). *Hierarchical modeling and analysis for spatial data*. Chapman & Hall/CRC. <https://doi.org/10.1201/b17115>
- Banerjee, S., Gelfand, A. E., Finley, A. O., & Sang, H. (2008). Gaussian predictive process models for large spatial data sets. *Journal of the Royal Statistical Society: Series B (Statistical Methodology)*, 70(4), 825–848. <https://doi.org/10.1111/j.1467-9868.2008.00663.x>
- Berk, R. H. (1966). Limiting behavior of posterior distributions when the model is incorrect. *The Annals of Mathematical Statistics*, 37(1), 51–58. <https://doi.org/10.1214/aoms/1177699597>
- Besag, J. (1974). Spatial interaction and the statistical analysis of lattice systems. *Journal of the Royal Statistical Society: Series B (Methodological)*, 36(2), 192–225. <https://doi.org/10.1111/j.2517-6161.1974.tb00999.x>
- Carpenter, B., Gelman, A., Hoffman, M. D., Lee, D., Goodrich, B., Betancourt, M., Brubaker, M., Guo, J., Li, P., & Riddell, A. (2017). Stan: A probabilistic programming language. *Journal of Statistical Software*, 76(1). <https://doi.org/10.18637/jss.v076.i01>
- Chandler, R. E., & Bate, S. (2007). Inference for clustered data using the independence loglikelihood. *Biometrika*, 94(1), 167–183. <https://doi.org/10.1093/biomet/asm015>
- Cox, D. R., & Reid, N. (2004). A note on pseudolikelihood constructed from marginal densities. *Biometrika*, 91(3), 729–737. <https://doi.org/10.1093/biomet/91.3.729>
- Cressie, N., & Johannesson, G. (2008). Fixed rank Kriging for very large spatial data sets. *Journal of the Royal Statistical Society: Series B (Statistical Methodology)*, 70(1), 209–226. <https://doi.org/10.1111/j.1467-9868.2007.00633.x>
- Davison, A. C., Padoan, S. A., & Ribatet, M. (2012). Statistical modeling of spatial extremes. *Statistical Science*, 27(2), 161–186. <https://doi.org/10.1214/11-STS376>
- Davison, A. C., Huser, R., & Thibaud, E. (2019). Spatial extremes. In A. E. Gelfand, M. Fuentes, J. A. Hoeting, & R. L. Smith (Eds.), *Handbook of environmental and ecological statistics* (pp. 711–744). Chapman; Hall/CRC.
- Diggle, P. J., Tawn, J. A., & Moyeed, R. A. (1998). Model-based geostatistics. *Journal of the Royal Statistical Society: Series C (Applied Statistics)*, 47(3), 299–350. <https://doi.org/10.1111/1467-9876.00113>
- Eidsvik, J., Shaby, B. A., Reich, B. J., Wheeler, M., & Niemi, J. (2014). Estimation and prediction in spatial models with block composite likelihoods. *Journal of Computational and Graphical Statistics*, 23(2), 295–315. <https://doi.org/10.1080/10618600.2012.760460>

- Fuglstad, G.-A., Simpson, D., Lindgren, F., & Rue, H. (2019). Constructing priors that penalize the complexity of Gaussian random fields. *Journal of the American Statistical Association*, 114(525), 445–452. <https://doi.org/10.1080/01621459.2017.1415907>
- Gelfand, A. E., Diggle, P. J., Fuentes, M., & Guttorp, P. (2010). *Handbook of spatial statistics*. CRC press. <https://doi.org/10.1201/9781420072884>
- Gneiting, T., & Raftery, A. E. (2007). Strictly proper scoring rules, prediction, and estimation. *Journal of the American Statistical Association*, 102(477), 359–378. <https://doi.org/10.1198/016214506000001437>
- Godambe, V. P. (1960). An optimum property of regular maximum likelihood estimation. *The Annals of Mathematical Statistics*, 31(4), 1208–1211. Retrieved April 22, 2022, from <http://www.jstor.org/stable/2237819>
- Heffernan, J. E., & Resnick, S. I. (2007). Limit laws for random vectors with an extreme component. *The Annals of Applied Probability*, 17(2), 537–571. <https://doi.org/10.1214/105051606000000835>
- Heffernan, J. E., & Tawn, J. A. (2004). A conditional approach for multivariate extreme values (with discussion). *Journal of the Royal Statistical Society: Series B (Statistical Methodology)*, 66(3), 497–546. <https://doi.org/10.1111/j.1467-9868.2004.02050.x>
- Hrafnkelsson, B., Siegert, S., Huser, R., Bakka, H., & Jóhannesson, Á. V. (2021). Max-and-Smooth: A two-step approach for approximate Bayesian inference in latent Gaussian models. *Bayesian Analysis*, 16(2), 611–638. <https://doi.org/10.1214/20-BA1219>
- Huser, R., & Wadsworth, J. L. (2022). Advances in statistical modeling of spatial extremes. *WIREs Computational Statistics*, 14(1), e1537. <https://doi.org/10.1002/wics.1537>
- Ingebrigtsen, R., Lindgren, F., & Steinsland, I. (2014). Spatial models with explanatory variables in the dependence structure. *Spatial Statistics*, 8, 20–38. <https://doi.org/10.1016/j.spasta.2013.06.002>
- Ingebrigtsen, R., Lindgren, F., Steinsland, I., & Martino, S. (2015). Estimation of a non-stationary model for annual precipitation in southern Norway using replicates of the spatial field. *Spatial Statistics*, 14, 338–364. <https://doi.org/10.1016/j.spasta.2015.07.003>
- Jóhannesson, Á. V., Siegert, S., Huser, R., Bakka, H., & Hrafnkelsson, B. (2022). Approximate Bayesian inference for analysis of spatiotemporal flood frequency data. *The Annals of Applied Statistics*, 16(2), 905–935. <https://doi.org/10.1214/21-AOAS1525>
- Kaufman, C. G., Schervish, M. J., & Nychka, D. W. (2008). Covariance tapering for likelihood-based estimation in large spatial data sets. *Journal of the American Statistical Association*, 103(484), 1545–1555. <https://doi.org/10.1198/016214508000000959>
- Keef, C., Papastathopoulos, I., & Tawn, J. A. (2013). Estimation of the conditional distribution of a multivariate variable given that one of its components is large: Additional constraints for the Heffernan and Tawn model. *Journal of Multivariate Analysis*, 115, 396–404. <https://doi.org/10.1016/j.jmva.2012.10.012>
- Keef, C., Tawn, J. A., & Lamb, R. (2013). Estimating the probability of widespread flood events. *Environmetrics*, 24(1), 13–21. <https://doi.org/10.1002/env.2190>
- Kleijn, B., & van der Vaart, A. (2012). The Bernstein-Von-Mises theorem under misspecification. *Electronic Journal of Statistics*, 6, 354–381. <https://doi.org/10.1214/12-EJS675>
- Kullback, S., & Leibler, R. A. (1951). On information and sufficiency. *The Annals of Mathematical Statistics*, 22(1), 79–86. <http://www.jstor.org/stable/2236703>
- Lindgren, F., & Rue, H. (2015). Bayesian spatial modelling with R-INLA. *Journal of Statistical Software*, 63(19), 1–25. <https://doi.org/10.18637/jss.v063.i19>
- Lindgren, F., Rue, H., & Lindström, J. (2011). An explicit link between Gaussian fields and Gaussian Markov random fields: The stochastic partial differential equation approach. *Journal of the Royal Statistical Society: Series B (Statistical Methodology)*, 73(4), 423–498. <https://doi.org/10.1111/j.1467-9868.2011.00777.x>
- Lindsay, B. G. (1988). Composite likelihood methods. *Contemporary mathematics*, 80(1), 221–239.

- Liu, Y., & Tawn, J. A. (2014). Self-consistent estimation of conditional multivariate extreme value distributions. *Journal of Multivariate Analysis*, 127, 19–35. <https://doi.org/10.1016/j.jmva.2014.02.003>
- Lombardo, L., Opitz, T., Ardizzone, F., Guzzetti, F., & Huser, R. (2020). Space-time landslide predictive modelling. *Earth-Science Reviews*, 209, 103318. <https://doi.org/10.1016/j.earscirev.2020.103318>
- Lumley, T., & Heagerty, P. (1999). Weighted empirical adaptive variance estimators for correlated data regression. *Journal of the Royal Statistical Society: Series B (Statistical Methodology)*, 61(2), 459–477. <https://doi.org/10.1111/1467-9868.00187>
- Marin, J.-M., Pudlo, P., Robert, C. P., & Ryder, R. J. (2012). Approximate Bayesian computational methods. *Statistics and Computing*, 22(6), 1167–1180. <https://doi.org/10.1007/s11222-011-9288-2>
- Opitz, T., Bakka, H., Huser, R., & Lombardo, L. (2022). High-resolution Bayesian mapping of landslide hazard with unobserved trigger event. *The Annals of Applied Statistics*, 16(3), 1653–1675. <https://doi.org/10.1214/21-AOAS1561>
- Opitz, T., Huser, R., Bakka, H., & Rue, H. (2018). INLA goes extreme: Bayesian tail regression for the estimation of high spatio-temporal quantiles. *Extremes*, 21(3), 441–462. <https://doi.org/10.1007/s10687-018-0324-x>
- Pauli, F., Racugno, W., & Ventura, L. (2011). Bayesian composite marginal likelihoods. *Statistica Sinica*, 21(1), 149–164. <http://www.jstor.org/stable/24309266>
- Ribatet, M., Cooley, D., & Davison, A. C. (2012). Bayesian inference from composite likelihoods, with an application to spatial extremes. *Statistica Sinica*, 22(2), 813–845. <http://www.jstor.org/stable/24310036>
- Richards, J., Tawn, J. A., & Brown, S. (2022). Modelling extremes of spatial aggregates of precipitation using conditional methods. *The Annals of Applied Statistics*, 16(4), 2693–2713. <https://doi.org/10.1214/22-AOAS1609>
- Rue, H., Martino, S., & Chopin, N. (2009). Approximate Bayesian inference for latent Gaussian models by using integrated nested Laplace approximations. *Journal of the Royal Statistical Society: Series B (Statistical Methodology)*, 71(2), 319–392. <https://doi.org/10.1111/j.1467-9868.2008.00700.x>
- Rue, H., Riebler, A., Sørbye, S. H., Illian, J. B., Simpson, D. P., & Lindgren, F. K. (2017). Bayesian computing with INLA: A review. *Annual Review of Statistics and Its Application*, 4(1), 395–421. <https://doi.org/10.1146/annurev-statistics-060116-054045>
- Shooter, R., Tawn, J., Ross, E., & Jonathan, P. (2021). Basin-wide spatial conditional extremes for severe ocean storms. *Extremes*, 24(2), 241–265. <https://doi.org/10.1007/s10687-020-00389-w>
- Simpson, D., Rue, H., Riebler, A., Martins, T. G., & Sørbye, S. H. (2017). Penalising model component complexity: A principled, practical approach to constructing priors. *Statistical Science*, 32(1), 1–28. <https://doi.org/10.1214/16-STS576>
- Simpson, E. S., Opitz, T., & Wadsworth, J. L. (2020). High-dimensional modeling of spatial and spatio-temporal conditional extremes using INLA and Gaussian Markov random fields [doi: 10.48550/arxiv.2011.04486]. <https://doi.org/10.48550/arxiv.2011.04486>
- Simpson, E. S., & Wadsworth, J. L. (2021). Conditional modelling of spatio-temporal extremes for Red Sea surface temperatures. *Spatial Statistics*, 41, 100482. <https://doi.org/10.1016/j.spasta.2020.100482>
- Sisson, S. A., Fan, Y., & Beaumont, M. (2018). *Handbook of approximate Bayesian computation*. CRC Press.
- Syring, N., & Martin, R. (2018). Calibrating general posterior credible regions. *Biometrika*, 106(2), 479–486. <https://doi.org/10.1093/biomet/asy054>
- Vandekog, S. M., Martino, S., Castro-Camilo, D., & Rue, H. (2022). Modelling sub-daily precipitation extremes with the blended generalised extreme value distribution. *Journal of Agricultural, Biological and Environmental Statistics*. <https://doi.org/10.1007/s13253-022-00500-7>
- Varin, C., Reid, N., & Firth, D. (2011). An overview of composite likelihood methods. *Statistica Sinica*, 21(1), 5–42. <http://www.jstor.org/stable/24309261>

- Vecchia, A. V. (1988). Estimation and model identification for continuous spatial processes. *Journal of the Royal Statistical Society: Series B (Methodological)*, 50(2), 297–312. <https://doi.org/10.1111/j.2517-6161.1988.tb01729.x>
- Wadsworth, J., & Tawn, J. (2022). Higher-dimensional spatial extremes via single-site conditioning. *Spatial Statistics*, 51, 100677. <https://doi.org/10.1016/j.spasta.2022.100677>
- Walker, S. G. (2013). Bayesian inference with misspecified models. *Journal of Statistical Planning and Inference*, 143(10), 1621–1633. <https://doi.org/10.1016/j.jspi.2013.05.013>
- White, H. (1982). Maximum likelihood estimation of misspecified models. *Econometrica*, 50(1), 1–25. <http://www.jstor.org/stable/1912526>

Supplementary material

S1 Implementing the spatial conditional extremes model in R-INLA

We implement the conditional extremes model,

$$[Y(\mathbf{s}) \mid Y(\mathbf{s}_0) = y_0 > t] \stackrel{d}{=} a(\mathbf{s}; \mathbf{s}_0, y_0) + b(\mathbf{s}; \mathbf{s}_0, y_0)Z(\mathbf{s}; \mathbf{s}_0) + \epsilon(\mathbf{s}; \mathbf{s}_0), \quad (\text{S1.1})$$

in R-INLA. Here, $Z(\mathbf{s}; \mathbf{s}_0)$ is a constrained Gaussian Matérn field and $\epsilon(\mathbf{s}; \mathbf{s}_0)$ is constrained Gaussian white noise. See Section 3 for more information.

R-INLA performs inference on latent Gaussian models of the form

$$\begin{aligned} [y_i \mid \mathbf{u}, \boldsymbol{\theta}_1] &\stackrel{i.i.d.}{\sim} \pi(y_i \mid \boldsymbol{\eta}(\mathbf{u}), \boldsymbol{\theta}_1), \quad i = 1, 2, \dots, n, \\ [\mathbf{u} \mid \boldsymbol{\theta}_2] &\sim \mathcal{N}(\boldsymbol{\mu}(\boldsymbol{\theta}_2), \mathbf{Q}^{-1}(\boldsymbol{\theta}_2)), \\ (\boldsymbol{\theta}_1, \boldsymbol{\theta}_2)^T &\sim \pi(\boldsymbol{\theta}_1)\pi(\boldsymbol{\theta}_2), \end{aligned}$$

where \mathbf{u} is a latent Gaussian field with mean $\boldsymbol{\mu}(\boldsymbol{\theta}_2)$ and precision matrix $\mathbf{Q}(\boldsymbol{\theta}_2)$. Hyperparameters $\boldsymbol{\theta} = (\boldsymbol{\theta}_1, \boldsymbol{\theta}_2)^T$, are assigned priors $\pi(\boldsymbol{\theta}_1)$ and $\pi(\boldsymbol{\theta}_2)$. Observations $\mathbf{y} = (y_1, \dots, y_n)^T$ are linked to the latent field through the linear predictor $\boldsymbol{\eta}(\mathbf{u}) = \mathbf{A}\mathbf{u}$, where \mathbf{A} is a known design matrix. This linear predictor defines the location parameter of the likelihood, via a possibly non-linear link function. In the R-INLA implementation, the observations are assumed to be conditionally independent given $\boldsymbol{\eta}$ and $\boldsymbol{\theta}_1$, so that $\pi(\mathbf{y} \mid \boldsymbol{\eta}(\mathbf{u}), \boldsymbol{\theta}_1) = \prod_i \pi(y_i \mid \eta_i(\mathbf{u}), \boldsymbol{\theta}_1)$. As mentioned in Section 1, the likelihood must be chosen from a predefined set of likelihood functions and the R-INLA user cannot modify it. The linear predictor can be decomposed into $d \geq 1$ components, $\boldsymbol{\eta}(\mathbf{u}) = \mathbf{A}^{(1)}\mathbf{u}^{(1)} + \dots + \mathbf{A}^{(d)}\mathbf{u}^{(d)}$, where each component represents, e.g., an intercept term, a linear combination of regression coefficients, an SPDE component, etc. All of these components must either be predefined in R-INLA or defined by the user, using the `rgeneric` framework or the recently added `cgeneric` framework.

The model in (S1.1) corresponds to a latent Gaussian model where the likelihood is Gaussian with variance θ_1 and the linear predictor is equal to $a(\mathbf{s}; \mathbf{s}_0, y_0) + b(\mathbf{s}; \mathbf{s}_0, y_0)Z(\mathbf{s}; \mathbf{s}_0)$,

where $\boldsymbol{\theta}_2$ contains the parameters of $a(\cdot)$, $b(\cdot)$ and $Z(\cdot)$. In our implementation we use the **cgeneric** framework to define the linear predictor as a sum of the two components $a(\mathbf{s}; \mathbf{s}_0, y_0)$ (see Section S1.2) and $b(\mathbf{s}; \mathbf{s}_0, y_0)Z(\mathbf{s}; \mathbf{s}_0)$ (see Section S1.1).

E. S. Simpson et al. (2020) employ the **rgeneric** model for implementing their version of the spatial conditional extremes model in R-INLA. However, **rgeneric** is considerably slower than **cgeneric**, which did not yet exist at the time of their work. The addition of the **cgeneric** framework in R-INLA allows us to implement a wide selection of forms for $a(\cdot)$ and $b(\cdot)$ at a lower computational cost.

S1.1 Implementing $b(\mathbf{s}; \mathbf{s}_0, y_0)Z(\mathbf{s}; \mathbf{s}_0)$ in R-INLA

In the following we describe how to implement the constrained, non-stationary field $b(\mathbf{s}; \mathbf{s}_0, y_0)Z(\mathbf{s}; \mathbf{s}_0)$ using the **cgeneric** framework. We first describe how to implement a non constrained non-stationary field and then how to include the constrain.

The stochastic partial differential equation (SPDE) approach of Lindgren et al. (2011) creates a Gaussian Markov random field $\hat{Z}(\mathbf{s})$ that is an approximation to a Gaussian random field $Z(\mathbf{s})$ with Matérn covariance function:

$$\text{Cov}(Z(\mathbf{s}), Z(\mathbf{s}')) = \frac{\sigma^2}{2^{\nu-1}\Gamma(\nu)} (\kappa \|\mathbf{s} - \mathbf{s}'\|)^\nu K_\nu(\kappa \|\mathbf{s} - \mathbf{s}'\|),$$

where σ^2 is the marginal variance, $\nu > 0$ is the smoothness parameter and $\rho = \sqrt{8\nu}/\kappa$ is the range parameter of $Z(\mathbf{s})$. Furthermore, K_ν is the modified Bessel function of the second kind and order ν . The smoothness parameter ν is difficult to estimate from data and is therefore often given a fixed value (Lindgren & Rue, 2015). The SPDE approximation $\hat{Z}(\mathbf{s})$ is constructed as a linear combination of Gaussian Markov random variables on a triangular mesh:

$$\hat{Z}(\mathbf{s}) = \sum_{i=1}^n \phi_i(\mathbf{s})W_i \stackrel{d}{\approx} Z(\mathbf{s}),$$

where W_1, \dots, W_n are Gaussian Markov random variables, and ϕ_i, \dots, ϕ_n are piecewise linear basis functions. Helper functions for creating the triangular mesh and the precision matrix of $\mathbf{W} = (W_1, W_2, \dots, W_n)^T$ are available in R-INLA. In order to approximate the non-stationary Gaussian random field $b(\mathbf{s}; \mathbf{s}_0, y_0)Z(\mathbf{s})$ with the SPDE approach, for any function $b(\mathbf{s}; \mathbf{s}_0, y_0)$, we modify the weights W_i to get

$$\hat{Z}_b(\mathbf{s}; \mathbf{s}_0, y_0) = \sum_{i=1}^n \phi_i(\mathbf{s})b(\mathbf{s}_i; \mathbf{s}_0, y_0)W_i \stackrel{d}{\approx} b(\mathbf{s}; \mathbf{s}_0, y_0)Z(\mathbf{s}), \quad (\text{S1.2})$$

where $\mathbf{s}_1, \dots, \mathbf{s}_n$ are the locations of the n Gaussian weights in the triangular mesh. This idea shares some similarities with the approach of Ingebrigtsen et al. (2014), Ingebrigtsen et al. (2015) for implementing non-stationary SPDE fields.

Since $\hat{Z}_b(\cdot)$ is created as a linear combination of Gaussian random variables, its variance equals

$$\text{Var} \left(\hat{Z}_b(\mathbf{s}; \mathbf{s}_0, y_0) \right) = \sum_{i,j=1}^n \phi_i(\mathbf{s}) \phi_j(\mathbf{s}) b(\mathbf{s}_i; \mathbf{s}_0, y_0) b(\mathbf{s}_j; \mathbf{s}_0, y_0) \text{Cov}(W_i, W_j),$$

which in general is unequal to

$$\text{Var}(b(\mathbf{s}; \mathbf{s}_0, y_0)Z(\mathbf{s})) = b(\mathbf{s}; \mathbf{s}_0, y_0)^2 \sigma^2.$$

However, if $\mathbf{s} = \mathbf{s}_i$ for $i = 1, 2, \dots, n$, then $\phi_i = 1$ while the other basis functions equal zero, resulting in a variance of

$$\text{Var} \left(\hat{Z}_b(\mathbf{s}; \mathbf{s}_0, y_0) \right) = b(\mathbf{s}; \mathbf{s}_0, y_0)^2 \text{Var}(W_i),$$

which is much closer to the correct variance. On the other hand, if $b(\mathbf{s}; \mathbf{s}_0, y_0)$ changes quickly and \mathbf{s} is far away from a mesh node, then the variance of $\hat{Z}_b(\mathbf{s}; \mathbf{s}_0, y_0)$ can be considerably different from the variance of $b(\mathbf{s}; \mathbf{s}_0, y_0)Z(\mathbf{s})$. Thus, if the mesh used for defining $\hat{Z}_b(\cdot)$ is dense and all data locations in \mathcal{S} are close to a mesh node, $\hat{Z}_b(\cdot)$ can provide a good approximation to $b(\mathbf{s}; \mathbf{s}_0, y_0)Z(\mathbf{s})$, but if the mesh is too coarse, the approximation may deteriorate in performance. It is a commonly known problem that using a too coarse mesh when approximating Gaussian random fields with the SPDE approach is problematic. This is also demonstrated in the simulation study in Section 4.2. However, the addition of a possible nonlinear function $b(\cdot)$, which turns the Gaussian random field into a nonstationary random field, makes the requirements on the mesh even stricter. Users of the SPDE approach should therefore be aware that a mesh that is good enough for approximating a stationary Gaussian field $Z(\mathbf{s})$ might not be good enough for approximating the non-stationary Gaussian field $b(\mathbf{s}; \mathbf{s}_0, y_0)Z(\mathbf{s})$.

S1.1.1 Constraining the residual field

$\hat{Z}_b(\cdot)$ provides a good approximation to the unconstrained Gaussian random field $b(\mathbf{s}; \mathbf{s}_0, y_0)Z(\mathbf{s})$. However, in order to implement the conditional extremes model in R-INLA, we need to approximate the constrained field $b(\mathbf{s}; \mathbf{s}_0, y_0)Z(\mathbf{s}; \mathbf{s}_0)$, where $Z(\mathbf{s}_0; \mathbf{s}_0) = 0$ almost surely. Wadsworth and Tawn (2022) describe two different methods for turning an unconstrained Gaussian field $Z(\mathbf{s})$ into a constrained field $Z(\mathbf{s}; \mathbf{s}_0)$. The first is to constrain the field by conditioning: $Z(\mathbf{s}; \mathbf{s}_0) = [Z(\mathbf{s}) \mid Z(\mathbf{s}) = 0]$, and the second is to constrain by subtraction: $Z(\mathbf{s}; \mathbf{s}_0) = Z(\mathbf{s}) - Z(\mathbf{s}_0)$. Wadsworth and Tawn (2022) use the first method while E. S. Simpson et al. (2020) use the second method in their case study. We argue that constraining by subtraction provides unrealistic dependence structures, and should be avoided if other alternatives are available. A quick computation shows that if $Z(\mathbf{s})$ is a stationary random process, then

$$\lim_{c \rightarrow \infty} \text{Corr}(Z(c\mathbf{s}; \mathbf{s}_0), Z(-c\mathbf{s}; \mathbf{s}_0)) = \frac{1}{2}, \quad (\text{S1.3})$$

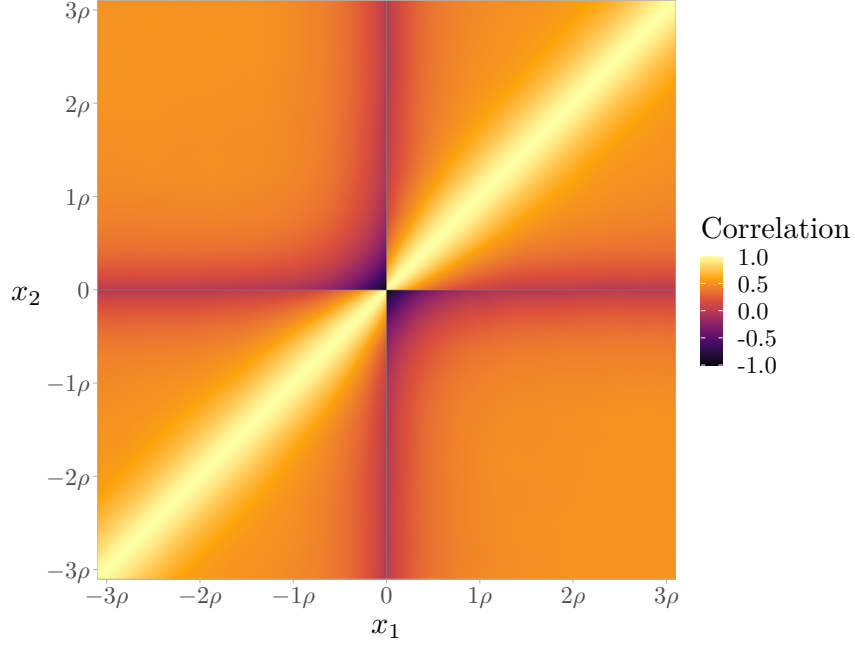


Figure S1.1: Correlation between $Z(\mathbf{s}_1; \mathbf{0})$ and $Z(\mathbf{s}_2; \mathbf{0})$, where $Z(\mathbf{s}; \mathbf{s}_0) = Z(\mathbf{s}) - Z(\mathbf{s}_0)$ and $Z(\mathbf{s})$ is a stationary Gaussian Matérn random field with range ρ and smoothness $\nu = 1.5$. Here, $\mathbf{s}_1 = (x_1, 0)^T$ and $\mathbf{s}_2 = (x_2, 0)^T$.

and if $Z(\mathbf{s})$ is isotropic with autocorrelation $\text{Corr}(Z(\mathbf{s}), Z(\mathbf{s}')) = r(\|\mathbf{s} - \mathbf{s}'\|)$, then

$$\text{Corr}(Z(\mathbf{s}_0 + \Delta\mathbf{s}; \mathbf{s}_0), Z(\mathbf{s}_0 - \Delta\mathbf{s}; \mathbf{s}_0)) = \frac{1 - 2r(\|\Delta\mathbf{s}\|) + r(2\|\Delta\mathbf{s}\|)}{2(1 - r(\|\Delta\mathbf{s}\|))}. \quad (\text{S1.4})$$

The limit of (S1.4) as $\|\Delta\mathbf{s}\| \rightarrow 0$ is often negative, and equals 0 for the exponential autocorrelation function and -1 for the Gaussian autocorrelation function. Thus, points that are infinitely far away from each other are strongly correlated while points that are infinitesimally close to each other might be negatively correlated or independent. Figure S1.1 displays the correlation structure of a Gaussian Matérn field that has been constrained by subtraction. This is clearly not a preferable correlation structure for most spatial processes.

R-INLA contains an implementation for constraining a random field by conditioning on linear combinations of itself (Rue et al., 2009). One can therefore easily constrain $\hat{Z}_b(\cdot)$ by conditioning using the `extraconstr` option in R-INLA. Unfortunately, this conditioning adds an extra computational cost that can become huge when dealing with high-dimensional spatial or spatio-temporal models. In practice, when using R-INLA with large data sets, we experienced that constraining by conditioning required more than ten times the amount of computer memory and computation time than constraining by subtraction. Constraining by conditioning therefore quickly turns infeasible for large data sets.

A third method for constraining the residual field is used by Richards et al. (2022). They model the variance of the residual field as a function of the distance $\|\mathbf{s} - \mathbf{s}_0\|$ such that the variance is zero when $\|\mathbf{s} - \mathbf{s}_0\| = 0$. This can easily be implemented by modifying the

standardising function $b(\cdot)$ in $\hat{Z}_b(\cdot)$ such that $b(\mathbf{s}_0; \mathbf{s}_0, y_0) = 0$. As an example, one can multiply $b(\mathbf{s}; \mathbf{s}_0, y_0)$ with the function

$$\sqrt{1 - \exp(-2\|\mathbf{s} - \mathbf{s}_0\|/\rho_b)},$$

where $\rho_b > 0$ can be either fixed or estimated. This expression is inspired by the variance of a conditional bivariate Gaussian distribution with exponential correlation function. In general, constraining $\hat{Z}_b(\cdot)$ by requiring that $b(\mathbf{s}_0; \mathbf{s}_0, y_0) = 0$ is almost as computationally efficient as constraining by subtraction, but without any of the undesirable properties discussed above. In our opinion one should therefore always prefer to constrain $\hat{Z}_b(\cdot)$ in this way when modelling spatial conditional extremes with R-INLA.

S1.2 Implementing $a(\mathbf{s}; \mathbf{s}_0, y_0)$ in R-INLA

Based on the R-INLA implementation of $b(\mathbf{s}; \mathbf{s}_0, y_0)Z(\mathbf{s}; \mathbf{s}_0)$ in Section S1.1, it might seem reasonable to simply represent the entire conditional extremes model using the SPDE approximation

$$\hat{Z}_{a,b}(\mathbf{s}; \mathbf{s}_0, y_0) = \sum_{i=1}^n \phi_i(\mathbf{s}) (a(\mathbf{s}_i; \mathbf{s}_0, y_0) + b(\mathbf{s}_i; \mathbf{s}_0, y_0)W_i) \stackrel{d}{\approx} a(\mathbf{s}; \mathbf{s}_0, y_0) + b(\mathbf{s}; \mathbf{s}_0, y_0)Z(\mathbf{s}).$$

However, this approximation has a mean equal to

$$\mathbb{E} \left[\hat{Z}_{a,b}(\mathbf{s}; \mathbf{s}_0, y_0) \right] = \sum_{i,j=1}^n \phi_i(\mathbf{s}) \phi_j(\mathbf{s}) a(\mathbf{s}_i; \mathbf{s}_0, y_0),$$

which in general is different from $a(\mathbf{s}; \mathbf{s}_0, y_0)$. Unlike in the previous section, there is a way of improving this approximation by representing $a(\cdot)$ using a separate random field that is independent of the SPDE approximation.

Given any deterministic vector \mathbf{a} , we claim that the Gaussian random field with mean \mathbf{a} and covariance matrix $\delta^2 \mathbf{I}$, where \mathbf{I} is the identity matrix and δ^2 is a fixed marginal variance close to zero, provides a good approximation to \mathbf{a} . Thus, we can approximate any standardising function $a(\mathbf{s}; \mathbf{s}_0, y_0)$ using a `cgeneric` model component with mean $a(\mathbf{s}; \mathbf{s}_0, y_0)$ and diagonal covariance matrix $\delta^2 \mathbf{I}$, where we set $\delta^2 = \exp(-15)$.

S2 A second simulation study with the spatial conditional extremes distribution

In the simulation study in Section 4.4, we found that, even though the adjustment method improved the frequency properties of the fitted conditional extremes models, it did not improve them as much as in the other three simulation studies in Section 4. In order to test our theory that this discrepancy is caused by self-inconsistency that complicates the

Table 6: Coverage percentages for unadjusted and adjusted credible intervals based on the composite conditional extremes likelihood with fixed ρ_b .

Aim	λ	λ_{adj}	κ	κ_{adj}	ρ	ρ_{adj}	σ	σ_{adj}	τ	τ_{adj}
90%	69%	91%	83%	88%	66%	87%	48%	88%	63%	87%
95%	77%	95%	89%	94%	70%	92%	53%	94%	74%	94%
99%	89%	98%	97%	99%	82%	98%	64%	97%	88%	97%

distribution of the simulated data, we perform a similar simulation study where we fit the spatial conditional extremes distribution to extremes of a Gaussian random process, instead of simulated data from the global conditional extremes distribution.

First, we define a rectangular grid, \mathcal{S} , with resolution 1×1 and size 15×15 . Then, we simulate data in \mathcal{S} using the SPDE approximation with variance $\sigma^2 = 1$ and range $\rho = 8$. Standardising the data to have Laplace marginals is easy, since the marginal distributions of the simulated data are known. We choose a threshold t equal to the 95% quantile of the Laplace distribution, and simulate data until we have observed 5×10^4 realisations such that each transformed realisation exceeds the threshold t in at least one location in \mathcal{S} . Then, we perform the pairwise parameter estimation procedure described in Section S3.2 to examine the best forms for $a(\mathbf{s}; \mathbf{s}_0, y_0)$ and $b(\mathbf{s}; \mathbf{s}_0, y_0)$ and to test whether the chosen forms from Section 4.4 can provide a reasonable fit to the transformed data.

The pairwise parameter estimation procedure shows that the parametric forms from Section 4.4 provide a good enough fit to the data, and using maximum likelihood estimation with the global composite likelihood, we find that the Kullback-Leibler distance (KLD; Kullback & Leibler, 1951) minimiser is

$$\boldsymbol{\theta}^* = (\lambda^*, \kappa^*, \sigma^*, \rho_b^*, \rho^*, \tau^*)^T \approx (3.9, 1.1, 1.4, 0.2, 6.8, 23.4)^T.$$

We evaluate the adjustment method by simulating 500 new realisation of the transformed Gaussian random field and fitting the global conditional extremes distribution to the available threshold exceedances with R-INLA. Then, the output from R-INLA is adjusted using the posterior adjustment method. This is repeated 300 times. The low value of ρ_b^* makes it difficult to estimate this parameter consistently, so we choose to fix the value of ρ_b to the estimated value of ρ_b^* during inference, and only compute posteriors for the five remaining parameters. Table 6 displays estimated coverage probabilities for how often the parameters in $\boldsymbol{\theta}^*$ are included in adjusted and unadjusted credible intervals. There is a considerable improvement for the adjusted credible intervals, and the overall frequency properties of the adjusted posteriors seem to be on par with those of the adjusted posteriors in Section 4.1, 4.2 and 4.3. The only differences between this simulation study and the one in Section 4.4 is that we simulated extreme data in different ways, and that we did not compute the posterior of ρ_b . However, we also repeat the simulation study from Section 4.4 where ρ_b is fixed and not estimated. The results are similar to those in Section 4.4: The adjusted posterior displays improved frequency properties, but these are not as good as in all other simulation

studies where we sample from self-consistent distributions. This implies that the observed problems in Section 4.4 are caused by the difficulties that arise when simulating data from a self-inconsistent distribution.

S3 Case study preliminaries

S3.1 Transforming the data to obtain Laplace marginals

The conditional extremes model in (S1.1) is defined for a random process with Laplace margins. However, most natural processes are not Laplace distributed. Thus, in order to perform inference with the conditional extremes model for a random process $X(\mathbf{s})$, one must first standardise it to a random process $Y(\mathbf{s})$ with Laplace margins. This is performed using the probability integral transform (Keef, Papastathopoulos, et al., 2013):

$$Y(\mathbf{s}) = \begin{cases} \log \{2F_{X(\mathbf{s})}(X(\mathbf{s}))\}, & X(\mathbf{s}) < F_{X(\mathbf{s})}(1/2) \\ -\log \{2[1 - F_{X(\mathbf{s})}(X(\mathbf{s}))]\}, & X(\mathbf{s}) \geq F_{X(\mathbf{s})}(1/2), \end{cases}$$

where $F_{X(\mathbf{s})}$ is the marginal distribution function of the random variable $X(\mathbf{s})$. We estimate the marginal distribution functions as the empirical distribution functions. However, independent standardisation of data at each location can lead to an unrealistic lack of smoothness in the transformed process $Y(\mathbf{s})$. Therefore, we apply a sliding window approach for computing the empirical distribution functions, where the distribution at location \mathbf{s} is estimated as the empirical distribution function of pooled data from all locations \mathbf{s}' such that $\|\mathbf{s} - \mathbf{s}'\| \leq r$ for some radius r . Based on exploratory analysis we find $r = 5$ km to yield a realistic degree of smoothness in the estimated marginal distributions of $X(\mathbf{s})$ (results not shown).

A problem with modelling precipitation is that the empirical distribution has a point mass in zero. This leads to $Y(\mathbf{s})$ having a truncated Laplace distribution with a point mass, which can cause problems during inference. In order for $Y(\mathbf{s})$ to follow a non-truncated Laplace distribution, we choose to remove all zeros from the process $X(\mathbf{s})$ and only focus on positive precipitation. This makes us unable to model the absence of precipitation, which can lead to overestimation of return levels for spatially aggregated precipitation. However, the main focus of this case study is to fit a Bayesian version of the spatial conditional extremes model to data and to improve the posterior with our adjustment method, and we do not focus on applying the fitted model for estimating properties of the untransformed process $X(\mathbf{s})$. We believe that our choices of removing all zeros and estimating marginals using empirical distribution functions of the positive precipitation values are acceptable given the aim of the current case study. More sophisticated transformations of the marginal distributions might be necessary if the aim is to predict or estimate properties of the untransformed process $X(\mathbf{s})$.

S3.2 Choosing models for $a(\mathbf{s}; \mathbf{s}_0, y_0)$ and $b(\mathbf{s}; \mathbf{s}_0, y_0)$

Due to the relatively small size of the domain \mathcal{S} , described in Section 5.1, we assume that the distribution of hourly precipitation data is approximately stationary over all locations in the sense that $a(\cdot)$, $b(\cdot)$, $Z(\cdot)$ and $\epsilon(\cdot)$ from (S1.1) are the same for all conditioning sites. We also assume that the data are isotropic and that $a(\mathbf{s}; \mathbf{s}_0, \cdot)$ and $b(\mathbf{s}; \mathbf{s}_0, \cdot)$ only depend on the distance $\|\mathbf{s} - \mathbf{s}_0\|$ between \mathbf{s} and \mathbf{s}_0 . Based on the suggestions and results of Richards et al. (2022), E. S. Simpson et al. (2020), and Wadsworth and Tawn (2022), we aim to model the precipitation data using the model in (S1.1) with standardising functions

$$\begin{aligned} a(\mathbf{s}; \mathbf{s}_0, y_0) &= \alpha(d) \cdot y_0 + \gamma(d), \\ b(\mathbf{s}; \mathbf{s}_0, y_0) &= \zeta(d) \cdot y_0^{\beta(d)}, \end{aligned} \quad d = \|\mathbf{s} - \mathbf{s}_0\|, \quad (\text{S3.1})$$

where $\alpha(d)$, $\gamma(d)$, $\zeta(d)$ and $\beta(d)$ are parametric functions with the constraints that $\alpha(0) = 1$, $\gamma(0) = 0$ and $\zeta(0) = 0$. Furthermore, $\alpha(d)$, $\gamma(d)$ and $\beta(d)$ are all assumed to converge to zero when the distance is so large that $Y(\mathbf{s})$ and $Y(\mathbf{s}_0)$ are independent. We also assume that the residual field $Z(\mathbf{s}; \mathbf{s}_0)$ is standardised to have zero mean and a variance of one.

Similarly to Richards et al. (2022), we get a sense of the best shape of the functions in (S3.1) for modelling our data, by first assuming that the residual field consists of Gaussian white noise, meaning that all observations are conditionally independent given $Y(\mathbf{s}_0)$. Two locations, \mathbf{s}_0 and \mathbf{s}_1 , are then drawn randomly from \mathcal{S} , and the conditional model

$$[Y(\mathbf{s}_1) \mid Y(\mathbf{s}_0) = y_0 > t] \stackrel{d}{=} \alpha \cdot y_0 + \gamma + \zeta \cdot y_0^\beta Z \quad (\text{S3.2})$$

is fitted to the observations from \mathbf{s}_0 and \mathbf{s}_1 , where Z is a standardised Gaussian random variable. This pairwise model fitting is repeated for 5000 random location pairs in \mathcal{S} . We set the threshold t equal to the 99.75% quantile of the Laplace distribution. This corresponds to an average of between one and three threshold exceedances per year of hourly summer data. In column 4 of Figure S3.1, the 5000 parameter estimates are displayed as functions of the distances between \mathbf{s}_1 and \mathbf{s}_0 . The parameter estimates are so full of noise that it is difficult to find any clear patterns. Consequently, we repeat the entire pairwise fitting procedure three more times while fixing either $\gamma = 0$, $\beta = 0$ or both $\gamma = 0$ and $\beta = 0$. This allows clearer patterns to emerge from the data (see the three remaining columns in Figure S3.1). Note that the parameter estimates in Figure S3.1 have been found using constrained optimisation, as unconstrained optimisation sometimes lead to estimates of ζ larger than 10^4 when both β and ζ are estimated simultaneously, and other similar problems. The constrained optimisation removes outliers like these to make it possible to extract useful information from the plots.

In order to choose parametric forms for the functions in (S3.1), we first note that it is possible for both $\gamma(d)$ and $\beta(d)$ to be constantly equal to zero. However, $\alpha(d)$ must decrease from $\alpha(0) = 1$ to $\alpha(\infty) = 0$, while $\zeta(d)$ must increase from $\zeta(0) = 0$ to $\zeta(d) > 0$ for $d > 0$. Therefore, we consider $\alpha(d)$ and $\zeta(d)$ to be the most fundamental parts of (S3.1), and in an attempt to get rid of the identifiability issues, we first choose parametric functions for

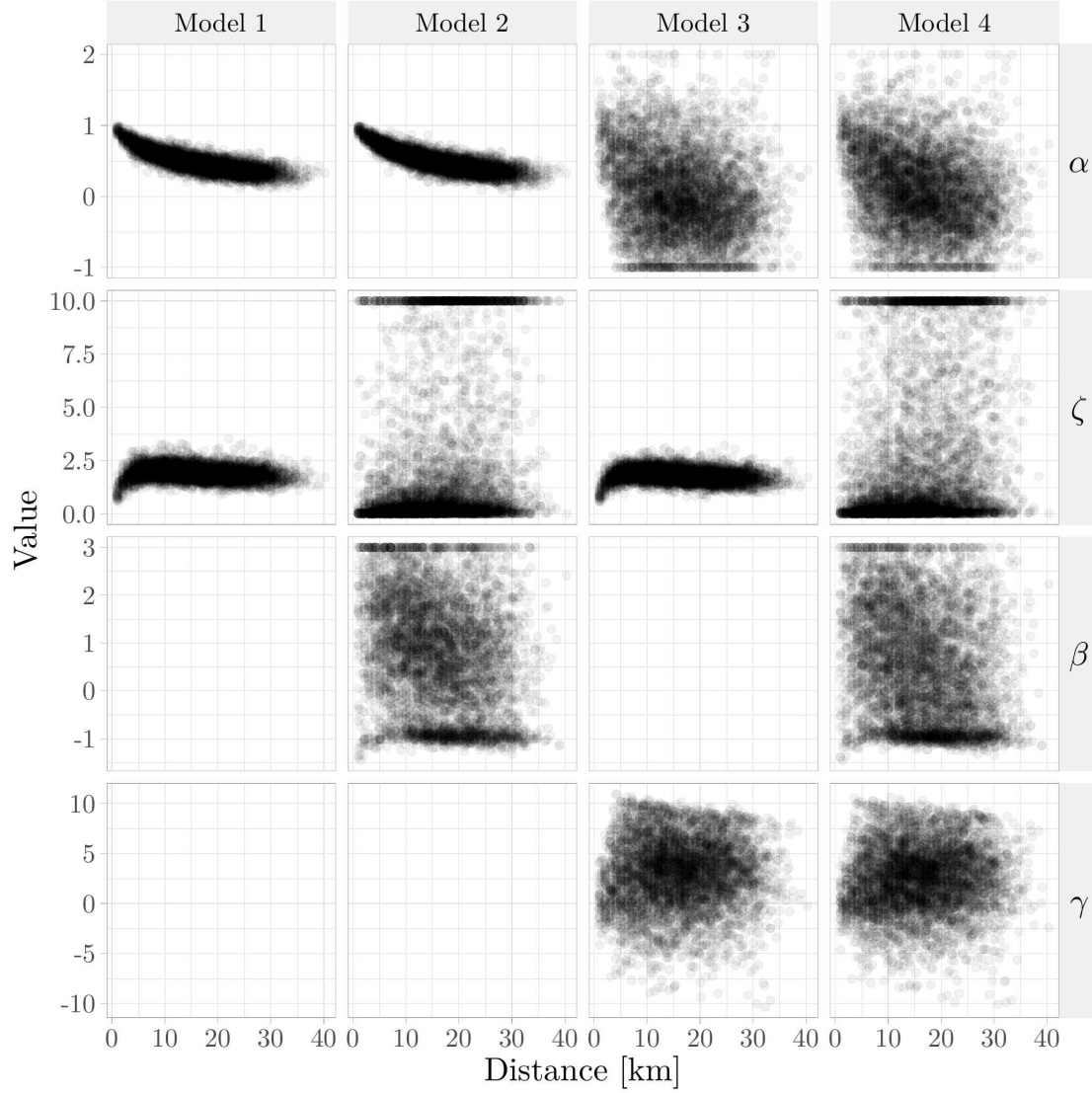


Figure S3.1: Parameter estimates from pairwise model fits using different pairs of \mathbf{s}_0 and \mathbf{s}_1 . Model 1 is model (S3.2) with fixed $\beta = \gamma = 0$. Model 2 is the same model with fixed $\gamma = 0$. Model 3 is the same model with fixed $\beta = 0$. Model 4 is the same model with all four parameters freely estimated.

$\alpha(d)$ and $\zeta(d)$ while we fix the functions $\gamma(d)$ and $\beta(d)$ equal to zero. The typical parametric choice for $\alpha(d)$ is

$$\alpha(d) = \exp \{ - (d/\lambda)^\kappa \},$$

with parameters $\lambda > 0$ and $\kappa > 0$ (Richards et al., 2022; Wadsworth & Tawn, 2022). This function corresponds well to the trends seen in Figure S3.1, so we choose it for modelling $\alpha(d)$. The pairwise estimates for $\zeta(d)$ shows that it is almost constant for large distances, and that it approaches zero for short distances. As discussed in Section S1.1.1, we therefore choose the parametric function

$$\zeta(d) = \sigma \sqrt{1 - \exp(-2d/\rho_b)},$$

with parameters $\sigma > 0$ and $\rho_b > 0$. The parameters of $\alpha(d)$ and $\zeta(d)$ are estimated using maximum likelihood estimation, where we still assume that the residual field consists of Gaussian white noise. The estimators $\hat{\alpha}(d)$ and $\hat{\zeta}(d)$ are displayed in the two leftmost subplots of Figure S3.2. They seem to agree well with the pairwise estimates from Figure S3.1.

Having estimated $\alpha(d)$ and $\zeta(d)$, we compute the residuals

$$\left[\frac{Y(\mathbf{s}_1) - \hat{\alpha}(\|\mathbf{s}_1 - \mathbf{s}_0\|)Y(\mathbf{s}_0)}{\hat{\zeta}(\|\mathbf{s}_1 - \mathbf{s}_0\|)} \mid Y(\mathbf{s}_0) > t \right], \quad (\text{S3.3})$$

for all 5000 pairs of \mathbf{s}_1 and \mathbf{s}_0 . We compute the mean and variance of these residuals, and find that the residual mean is close to zero, while the residual variance is close to one. The pairwise estimation procedure used for creating Figure S3.1 is then repeated on the residuals, in order to examine trends in $\gamma(d)$ and $\beta(d)$. Pairwise estimates of γ and β are displayed in the two rightmost subplots of Figure S3.2. The patterns in the pairwise estimates are weak, full of noise and centred around zero. Based on these findings we choose to set $\gamma(d) = \beta(d) = 0$ and we conclude that the spatial conditional extremes model with

$$\begin{aligned} a(\mathbf{s}; \mathbf{s}_0, y_0) &= \alpha(d) \cdot y_0 = y_0 \exp \{ - (d/\lambda)^\kappa \}, \\ b(\mathbf{s}; \mathbf{s}_0, y_0) &= \zeta(d) = \sigma \sqrt{1 - \exp(-2d/\rho_b)}, \end{aligned} \quad d = \|\mathbf{s} - \mathbf{s}_0\|, \quad (\text{S3.4})$$

provides a good enough fit to the data. We note that, clearly, $\zeta(d)$ does not provide a perfect fit to the trends of the pairwise estimates in Figure S3.1, and a better approximation would likely decrease slightly with the distance d . There are also still some weak trends remaining in the pairwise estimates for β . However, as mentioned in Section S3.1, our aim is not to estimate return levels or similar properties of the precipitation data, but simply to fit a Bayesian version of the spatial conditional extremes model to data and to improve the posterior using our adjustment method. The chosen models for $a(\mathbf{s}; \mathbf{s}_0, y_0)$ and $b(\mathbf{s}; \mathbf{s}_0, y_0)$ are therefore good enough for our intended goal, even though they might not be good enough for, e.g., reliable estimation of return levels.

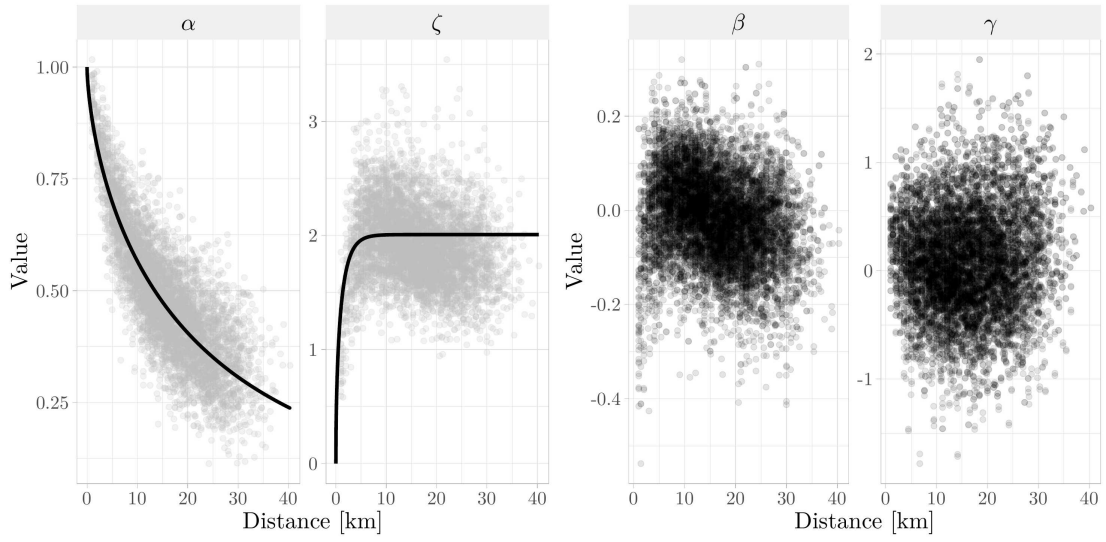


Figure S3.2: Left: Pairwise parameter estimates from column 1 of Figure S3.1, in grey, together with the maximum likelihood estimators of $\alpha(d)$ and $\zeta(d)$, displayed as black lines. Right: Pairwise parameter estimates of β and γ based on fitting the pairwise conditional extremes model (S3.2) to the residuals in (S3.3).